ORIGINAL PAPER

On new families of anisotropic spatial log-Gaussian Cox processes

Fariba Nasirzadeh[1] · Zohreh Shishebor[1] · Jorge Mateu[2]

Abstract

Cox processes are natural models for point process phenomena that are environmentally driven, but much less natural for phenomena driven primarily by interactions amongst the points. The class of log-Gaussian Cox processes (LGCPs) has an elegant simplicity, and one of its attractive features is the tractability of the multivariate normal distribution carries over, to some extent, to the associated Cox process. In the statistical analysis of spatial point patterns, it is often assumed isotropy because of a simpler interpretation and ease of analysis. However, there are many cases in which the spatial structure depends on the direction. In this paper, we introduce new families of anisotropic spatial LGCPs that are useful to model spatial anisotropic point patterns that exhibit a degree of clustering. We propose classes of families consisting of elliptical and non-elliptical models. The former can be reduced to isotropic forms after some rotations, while the latter family goes beyond this property. We derive analytical forms for the covariance of the associated random field, and some second-order characteristics. A moment-based estimation procedure is followed to make inference on the parameters that control the degree of anisotropy. The estimation procedure is evaluated through a simulation study under a variety of scenarios and various degrees of anisotropy. Our methodology is illustrated on two real datasets of earthquakes in South America and the Mediterranean Europe.

Keywords Anisotropy · Intensity function · *K*-function · Log-Gaussian Cox processes · Minimum contrast estimation · Pair correlation function · Super-ellipse

1 Introduction

An outstanding class of stochastic point processes is the class of spatial point processes, defined as random mechanisms to generate a countable set of points randomly located on, usually, a planar space. These processes are applied in many different fields such as geology, seismology, economics, image processing, ecology, or biology; see, as some Examples, Funwi-Gabga and Mateu (2012), Uria et al. (2013), Serra et al. (2014). The Poisson point process is the most basic and simplest model of point processes. This model can be used to build a more flexible and fundamental class of spatial models named Cox processes. A Cox process is obtained as an extension of a Poisson process by considering the intensity function of the Poisson process a realization of a random field. Cox processes are natural models for point process phenomena that are environmentally driven, but much less natural for phenomena driven primarily by interactions amongst the points.

The simplicity of using a Cox process lies in the fact that the moment properties of a Cox process are equivalent to the moment properties of its corresponding intensity random field. Indeed, in the stationary case, the intensity of a Cox process is equal to the expectation of the random field, and the covariance density of the Cox process is equal to the covariance function of the random intensity (Diggle et al. 2013). In addition, the *K*-function, which is the reduced second moment measure of a Cox process (Ripley 1976), is simply obtained through the covariance function of the underlying random field. This close relation between point process data and geostatistical data provides flexibility in terms of computation and when the spatial correlation is being analyzed.

✉ Zohreh Shishebor
    shisheb@shirazu.ac.ir

[1] Department of Statistics, Shiraz University, Shiraz, Iran

[2] Department of Mathematics, University Jaume I, Castellon, Spain

The literature offers some subclasses of Cox processes of particular interest. We can find Thomas processes (Thomas 1949), Neyman-Scott processes (Neyman and Scott 1958), Matérn cluster processes (Matérn 1960, 1986), shot noise Cox processes (Cox and Isham 1980), Poisson-gamma processes (Wolpert and Ickstadt 1998), shot noise G Cox processes (Brix 1999), and log-Gaussian Cox processes (Coles and Jones 1991; Møller et al. 1998). Møller et al. (1998) considered the class of log-Gaussian Cox processes (LGCPs) which is defined as a Cox process with random intensity $\Lambda(x) = \exp\{Z(x)\}$, where Z is a Gaussian process. The reader is referred to Sect. 5 of Møller and Waagepetersen (2003) for a deeper treatment of these subclasses.

The log-Gaussian construction has an elegant simplicity. One of its attractive features is that the tractability of the multivariate Normal distribution carries over, to some extent, to the associated Cox process. Diggle et al. (2013) described the class of LGCPs as models for spatial and spatio-temporal point process data, and suggested a more useful definition of geostatistics. They noted that a LGCP is a natural analog for point process data of the linear Gaussian model for real-valued geostatistical data. In line with the linear Gaussian model, the LGCP class lacks any mechanistic interpretation. Its principal virtue is that it provides a flexible and relatively tractable class of empirical models for describing spatially correlated phenomena. This makes it extremely useful in a range of applications where the scientific focus is on spatial prediction rather than on testing mechanistic hypotheses.

Under ergodicity, a point process is stationary and isotropic, if its statistical properties do not change under translation and rotation, respectively. Informally, *stationarity* implies that one can estimate properties of the process from a single realization, by exploiting the fact that these properties are the same in different, but geometrically similar, subregions of the spatial domain; *isotropy* means that there are no directional effects. The condition of isotropy is often made in practice as a pragmatic assumption to ease the statistical analysis. However, this assumption is not realistic and it is not satisfied in many real applications, and failure to account for spatial and directional inhomogeneity can result in erroneous inferences. A spatial point pattern is called anisotropic if its spatial structure depends on direction.

Directional analysis has mainly been concentrated on two types of anisotropy, geometric anisotropy, where anisotropy is caused by a linear transformation of a stationary and isotropic process, and increased intensity of points along directed lines. Here, we are explicitly interested in those spatial point patterns with second-order statistical characteristics that depend on particular angles and directions. Anisotropy can be present when the spatial point patterns contain points placed roughly on line segments. See details in Møller and Rasmussen (2012) who consider a particular class of point processes whose realizations contain such linear structures.

Osher and Stoyan (1981) presented a method for the second-order analysis of anisotropic point processes. They provided expressions for the anisotropic spatial K-function, and used this function to define an orientation distribution function. Guan et al. (2004, 2006) proposed a formal nonparametric approach to test for isotropy based on the asymptotic joint normality of the sample second-order intensity function. Alternative methods based on two-dimensional spectral analysis were proposed by Mugglestone and Renshaw (1998). The complications inherent with spectral analysis (particularly for more than one dimension) appear to have discouraged applied statisticians and ecologists from making use of these methods. Wavelet analysis has succeeded in a variety of applications and held promise in the area of spatial pattern analysis (Donoho 1993; Gao and Li 1993; Grenfell et al. 2001). However, wavelet analysis has only been involved in several works for the detection of spatial patterns (Harper et al. 2001; Perry et al. 2002; Rosenberg 2004). In general, there is not a large treatment of anisotropy for spatial planar point patterns, and there is currently only one such approach for three-dimensional point patterns (Redenbach et al. 2009). All these references are very much focussed on anisotropy for spatial point processes, which is our focus. However, and due to the link between LGCPs and geostatistics, there are also a number of contributions acting directly on the covariance structure of the Gaussian Random Field; we refer the reader to different classes of anisotropic covariance functions appeared in Allard et al. (2016), Fuglstad et al. (2015), or Hristopulos (2012).

Except the contribution by Møller and Rasmussen (2012), the above mentioned papers (acting on spatial point processes) are more focused on testing anisotropy and describing main directions. However, in this paper, we are interested in point pattern models for anisotropic behaviors, and in this sense the literature is scarce. In particular, we highlight the contribution of Møller and Toftaker (2014) who proposed a new class of anisotropic Cox processes based on elliptical anisotropic pair correlation function models. They also showed that in such classes, by a rotation of the original vector coordinates, the anisotropic pair correlation function in the geometric class can be rewritten as an isotropic pair correlation function in a new system of coordinates. Using the rotation matrix is shown to be useful because it helps to simplify the calculations using isotropic models instead of anisotropic ones. However, this approach has two problems. First, it is usually complicated to obtain close analytical forms for the corresponding second-order summary statistics of the LGCP model. Second, it is

challenging to study non-elliptical and anisotropic covariance models that cannot be reduced to an isotropic form under a rotation.

Therefore, the main objective of our paper is to present a new integrated perspective on constructing LGCP models to overcome the above-mentioned challenges. Our methods can build anisotropic covariance models that belong to elliptical and non-elliptical classes of covariance functions. With the non-elliptical classes, we deviate from Møller and Toftaker (2014). We also present the elliptical ones as for them we are able to obtain close forms that Møller and Toftaker (2014) did not show. See "Appendix" A.

In particular, we develop new classes of anisotropic LGCPs while finding analytical forms for the covariance of the associated random field, $C(.)$, and for some second-order characteristics, the pair correlation, $g(.)$, and K-measure, $\kappa(A) = \int_A g(u)du$, where $A \subseteq \mathbb{R}^2$ is a bounded Borel set, and u is a generic location. Our idea lies on building an anisotropic covariance function. The diagram in Fig. 1 shows a scheme of our building block, which draws the basics of what is presented in Sect. 3.

The plan of the paper is as follows. Section 2 contains some basics of point processes and their properties. Section 3 presents our new classes of anisotropic LGCP models. Our method is shown to be used to build both elliptical and non-elliptical anisotropic models. Several examples are illustrated. Section 4 is devoted to the study of moment-based estimation of the anisotropic parameters, and a simulation study to investigate the performance of the estimation procedure comes in Sect. 5. Finally, in Sect. 6, we analyze two real datasets of earthquakes in South America and the Mediterranean Europe. The paper ends with some final conclusions and a discussion.

2 Notation and setup for point processes

Let X be a point process on $\mathbb{S} \subseteq \mathbb{R}^2$ specified by a so-called intensity function $\lambda : \mathbb{S} \to [0, \infty)$ which is locally integrable, i.e. $\int_B \lambda(\xi)d\xi < \infty$ for all bounded $B \subseteq \mathbb{S}$. For any subset $\aleph \subseteq \mathbb{S}$, let $n(\aleph)$ denote the cardinality of a point configuration $\aleph$, setting $n(\aleph) = \infty$ if $\aleph$ is not finite. Then the point process X takes values in the space defined by

$$N_\aleph = \{\aleph \subseteq \mathbb{S} : n(\aleph \cap B) < \infty \text{ for all bounded } B \subseteq \mathbb{S}\}.$$

For a point process X on $\mathbb{S}$, consider the counting function

$$N(B) = n(X \cap B)$$

which gives the random number of points falling in a bounded set $B \subseteq \mathbb{S}$. Throughout the paper, we use u and v to denote generic points in $\mathbb{S} \subseteq \mathbb{R}^2$, and the events of the point process X will be denoted by x.

The mean of the counts $N(B)$ is given by

$$E[N(B)] = \int_B \lambda(u)du,$$

which reduces to $\lambda|B|$ when λ is constant, and with $|B|$ indicating the area of B. In this case, X is said to be homogeneous, or stationary with intensity λ; otherwise X is said to be inhomogeneous. The variance $Var[N(B)]$ is defined through the second-order intensity function $\lambda^{(2)} : \mathbb{S} \times \mathbb{S} \to [0, \infty)$ as

$$Var[N(B)] = \int_B \int_B \lambda^{(2)}(u,v)dudv + \int_B \lambda(u)du(1 - \int_B \lambda(u)du).$$

For stationary processes, the variance of $N(B)$ takes the form $\int_B \int_B \lambda^{(2)}(u,v)dudv + \lambda|B|(1 - \lambda|B|)$. Also, the covariance function of $N(.)$ for bounded $A, B \subseteq \mathbb{S}$ is given by
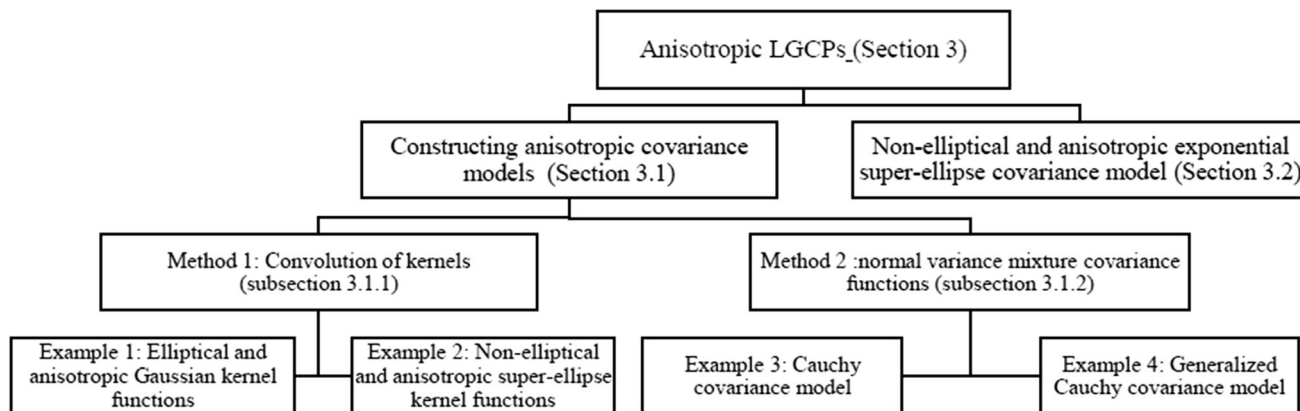

Fig. 1 A graphical summary of our proposal

$$Cov[N(A,)N(B)] = \int_A \int_B \lambda^{(2)}(u,v)dudv + \lambda|A \cap B| - \lambda^2|A||B|,$$

where $A \cap B$ denotes the intersection of A and B (Diggle 2013; Møller and Waagepetersen 2003).

If both λ and $\lambda^{(2)}$ exist, the pair correlation function, g, is defined by

$$g(u,v) = \lambda^{(2)}(u,v)/(\lambda(u)\lambda(v)),$$

using the convention $\frac{a}{0} = 0$ for $a \geq 0$. This scale function is not a usual correlation function. In the stationary case, g is reduced to $\lambda^{(2)}(u,v)/\lambda^2$ and it becomes translation invariant, i.e. $g(u,v) = g(u-v)$.

The most fundamental example of point processes is the Poisson point process with intensity function λ. For this process, for any $B \subseteq \mathbb{S}$, $N(B)$ follows a Poisson distribution with mean $\mu(B) = \int_B \lambda(u)du < \infty$, and for any $n \in N$ and $B \subseteq \mathbb{S}$, conditional on $N(B) = n$, $X \cap B$ has a Binomial distribution with probability function $f(x) = \lambda(x)/\mu(B)$. It is easily shown that the pair correlation function is equal to one, i.e. $g(u,v) = 1$ for a Poisson process. The proof comes from a direct consequence of the Slivnyak-Mecke theorem.

Here, we are interested in the flexible and fundamental class of Cox models. A Cox process is obtained as an extension of a Poisson process in the case that the intensity function of the Poisson process is considered a realization of a random field. Suppose that $\Lambda = \{\Lambda(x) : x \in \mathbb{S}\}$ is a non-negative random field. Conditional on the realization $\Lambda(x) = \lambda(x)$ with $x \in \mathbb{S}$, if the point process X is a Poisson process on S with intensity function Λ, then X is said to be a Cox process driven by Λ. A Cox process is said to be stationary if and only if its intensity is stationary, and similarly for isotropy. In the stationary case, the intensity of the Cox process is equal to the expectation of the intensity of the random field, i.e. $\lambda = E[\Lambda(x)]$, and the covariance density of the Cox process is equal to the covariance function of the random intensity, i.e., $C(u) = Cov\{\Lambda(x), \Lambda(x-u)\}$. This close relation between point process data and geostatistical data helps describing the spatial correlation. Also, the reduced second moment measure, or the K-function (Ripley 1976), of the Cox process is simply obtained as

$$K(\rho) = \pi\rho^2 + 2\pi\lambda^{-2} \int_0^\rho C(v)vdv,$$

where λ is the intensity of the Cox process and $C(v)$ is the covariance density of the Cox process. We note that the K-function of a Poisson point process over a disc takes the form $K(\rho) = \pi\rho^2$. The class of stationary log-Gaussian Cox processes (LGCPs) is defined as a Cox process with $\Lambda(x) = \exp\{Z(x)\}$, where Z is a Gaussian process with mean μ, variance σ^2 and correlation function $r(u)$ (Møller et al. 1998). It can be proved that such LGCP has intensity $\lambda = \exp\{\mu + 0.5\sigma^2\}$ and covariance density $C(u) = \lambda^2[\exp\{\sigma^2 r(u)\} - 1]$. Diggle et al. (2013) suggested to re-parameterize the model as $\Lambda(x) = \exp\{\gamma + Z(x)\}$, where $E[Z(x)] = -0.5\sigma^2$, so that $E[\exp\{Z(x)\}] = 1$ and $\lambda = \exp\{\gamma\}$. This re-parameterization gives a clean separation between first- and second-order properties.

So far most of the contributions in this context have limited their attention to the case where Λ is stationary and isotropic. However, these assumptions are not realistic in many real applications. This paper focuses on anisotropic models for which the distribution of Λ is not invariant under rotations.

3 Anisotropic LGCPs

Let X be a LGCP model driven by intensity function $\Lambda(x) = \exp\{Z(x)\}$. In constructing an anisotropic LGCP model, in terms of properties of the model, we need $Z(x)$ to have an anisotropic covariance function. We propose two strategies to obtain anisotropic LGCPs. The first one, presented in Sect. 3.1, builds anisotropic covariance functions through some mechanistic procedures based on kernels convolution and normal variance mixtures. The second strategy, presented in Sect. 3.2, provides a direct model of non-elliptical anisotropic covariance function that is plugged into the random field $Z(x)$. We note that both strategies can be used to build non-elliptical anisotropic models.

3.1 Constructing anisotropic covariance models through mechanistic procedures

3.1.1 Method 1: Convolution of kernels

Higdon et al. (1999) proposed an inhomogeneous spatial covariance function based on the convolution of two kernels centered at the locations of interest. We use this approach in the anisotropic case. In more detail, an inhomogenous and anisotropic spatial covariance function can be defined by the auto-convolution of an anisotropic kernel function. Then according to the properties of LGCPs, an anisotropic LGCP model can be obtained using an anisotropic covariance function. To do this, some anisotropic kernel functions can be used such as Gaussian kernel functions, Gaussian radial basis functions, Laplace RBF kernels, Cauchy kernel functions, Lame kernels, super-ellipse kernels, etc. The later type of kernel allows to construct non-elliptical covariance functions. In what follows, an anisotropic Gaussian kernel function is used as an

example of this approach to build an elliptical anisotropic covariance function. Additionally, an exponential super-ellipse kernel function is considered to build the non-elliptical anisotropic covariance function of the Gaussian process, which represents a new class of non-elliptical anisotropic LGCPs based on this covariance function. We emphasize that our main goal is to build anisotropic models based on anisotropic covariance functions for LGCPs, which makes a clear difference with the more geostatistical models in Higdon et al. (1999). Following Higdon et al. (1999), we can build an inhomogeneous covariance function based on the convolution of kernels centered at the locations of interest, as follows

$$C(x, y) = \int_{\mathbb{R}^2} k(x, v)k(y, v)dv, \tag{1}$$

where x, y and v are locations in $\mathbb{R}^2$, and k is a kernel function. It is easy to show that $C(x, y)$ is a non-negative definite function for spatially-varying kernel functions of any functional form.

Example 1 Elliptical and anisotropic Gaussian kernel functions

Here, the elliptical and anisotropic Gaussian kernel function is used in constructing the anisotropic covariance function of LGCP models. An anisotropic Gaussian kernel function has different kernel parameters per dimension instead of a single kernel parameter for all the elements. Let

$$k(x, y) = \exp\left\{-\sum_{m=1}^{2} \frac{(x_m - y_m)^2}{2\sigma_m}\right\}, \tag{2}$$

be such an anisotropic kernel function, where $x = (x_1, x_2)$ and $y = (y_1, y_2)$ are points in $\mathbb{R}^2$. For the anisotropic Gaussian kernel, each parameter σ_m is tuned separately.

Substituting (2) into (1) yields an anisotropic covariance function

$$C_{aniso}(x, y) = \pi\sqrt{\sigma_1\sigma_2}\exp\left\{-\sum_{m=1}^{2} \frac{(x_m - y_m)^2}{4\sigma_m}\right\}, \tag{3}$$

which can be written as

$$C_{aniso}(x, y) = \sigma^2\exp\left\{-(x - y)^{\tau}\Sigma^{-1}(x - y)\right\},$$

where $\sigma^2 = \pi\sqrt{\sigma_1\sigma_2}$ is the variance, and Σ is an anisotropic diagonal matrix with elements $(4\sigma_1, 4\sigma_2)$. This anisotropic covariance function can be written in terms of an isotropic exponential covariance function C_{iso} defined as $C_{iso}(v) = \sigma^2\exp\{-v\}$, using the following change of variables (but not through a rotation)

$$C_{aniso}(u) = C_{iso}(u^{\tau}\Sigma^{-1}u),$$

with u the separation vector of x and y. Finally, note that if Σ were the identity matrix, $C_{aniso} = C_{iso}$, but in our case, Σ is a diagonal matrix containing the anisotropic parameters. This covariance function belongs to the elliptical class of covariance models. Møller and Toftaker (2014) studied this class of covariance model using a suitable rotation to reduce it to an isotropic model. However, we consider our anisotropic LGCP model directly and without any rotation. The pair correlation function and the covariance function of a general LGCP have a one-to-one correspondence, and the former can be obtained from the latter.

Let X be a LGCP with intensity

$$\Lambda(x) = \exp\{Z(x)\},$$

where $Z(.)$ is a Gaussian process with mean μ, variance σ^2 and covariance function $C(\cdot)$. The first and second moments of $\Lambda(x)$ are obtained as $E[\Lambda(x)] = \exp\{\mu + \frac{1}{2}\sigma^2\}$, and $E[\Lambda(x)\Lambda(x - u)] = \exp\{2\mu + \sigma^2 + C(u)\}$, respectively. After rewriting the model as $\Lambda(x) = \exp\{\gamma + Z(x)\}$, $E[\exp\{Z(x)\}] = 1$ and $\lambda = \exp\{\gamma\}$, and this leads to the covariance function being reduced to $C(\Lambda(x), \Lambda(x - u)) = \exp\{C(u)\} - 1$; the pair correlation can be then written as

$$g(u) = \exp\{C(u)\}. \tag{4}$$

Substituting (3) into (4) we can obtain a close analytical form for the anisotropic pair correlation function, given by

$$g_{aniso}(u) = \exp\left\{\pi\sqrt{\sigma_1\sigma_2}\exp\left\{-\sum_{k=1}^{2}\frac{u_k^2}{4\sigma_k}\right\}\right\}. \tag{5}$$

Equivalently, (5) can be rewritten as

$$g_{aniso}(u) = \exp\{\sigma^2\exp\{-u^{\tau}\Sigma^{-1}u\}\}, \tag{6}$$

where again u is the separation vector of x and y, $\sigma^2 = \pi\sqrt{\sigma_1\sigma_2}$ and Σ is an anisotropic diagonal matrix with elements $(4\sigma_1, 4\sigma_2)$.

For a general anisotropic point process, a close relationship between the reduced second moment measure and the pair correlation function g is given by

$$\kappa(A) = \int_A g(u)du, \tag{7}$$

for a bounded set A (Baddeley et al. 2015). Following Illian et al. (2008) and Baddeley et al. (2015), A could be a disc, or a sector of a disc, which is the part of the disc of radius ρ lying between two lines at orientations θ_0 and θ_1. The use of sector K-function is also explained in Ohser and Stoyan (1981).

For completeness, assume A is a disc centred at the origin with radius ρ, denoted by $C(0, \rho)$ and analytically represented by $\|u\| \leq \rho$. Substituting (6) into (7), the anisotropic K-function over the disc A, denoted by K_{aniso}^{G}, is given by

$$K_{aniso}^{G}(\rho) = \int\limits_{\|u\| \leq \rho} \exp\{\pi\sqrt{\sigma_1\sigma_2}\exp\{-u^\tau\Sigma^{-1}u\}\}du \quad (8)$$

Example 2 Non-elliptical and anisotropic super-ellipse kernel functions

We consider here the class of separable kernel functions with one-dimensional components of the same functional form. This kernel function can not be reduced to isotropic functions under rotation. In a coordinate system aligned with the principal axes, these kernels are expressed as

$$k(u) = \sigma^2 \prod_{i=1}^{2} h(u_i), \quad (9)$$

where $h(.)$ is a permissible one-dimensional kernel function (Christakos 1992), σ^2 is a variance parameter, and $u = (u_1, u_2)$.

A family of separable kernel models was introduced by Hristopulos (2002) and it is defined in terms of geometrical generalizations of the ellipse, called super-ellipsoids (Wallace 1968). In two spatial dimensions a super-ellipsoid with index n obeys the following equation

$$\left|\frac{u_1}{\sigma_1}\right|^{\frac{2}{n}} + \left|\frac{u_2}{\sigma_2}\right|^{\frac{2}{n}} = |\tilde{u}_1|^{\frac{2}{n}} + |\tilde{u}_2|^{\frac{2}{n}} = \omega, \quad (10)$$

where $\tilde{u}_i = \frac{u_i}{\sigma_i}; i = 1, 2$. Analogous to a circle, a super-ellipse in (10) can be written as

$$S(\theta) = \begin{bmatrix} a\omega^{\frac{n}{2}}cos^n(\theta) \\ b\omega^{\frac{n}{2}}sin^n(\theta) \end{bmatrix}; \quad -\pi < \theta < \pi.$$

The exponent $S(\theta)$ with power n is a signed power function such that $cos^n(\theta) = sign(cos(\theta))|cos(\theta)|^n$.

We focus on the class of two dimensional super-ellipsoid kernel functions that can be reduced to one-dimensional components of the same kernel functional form with index n, given by

$$k(\tilde{u}) = \sigma^2 h\left(|\tilde{u}_1|^{\frac{2}{n}}\right) h\left(|\tilde{u}_2|^{\frac{2}{n}}\right), \quad (11)$$

where $\tilde{u} = (\tilde{u}_1, \tilde{u}_2)$.

Here, we are interested in using the exponential super-ellipsoid form as an important and known family of super-ellipsoid kernel functions. This family is defined as a particular case of (11)

$$k(\tilde{u}) = \sigma^2 \exp\left(-\left|\frac{u_1}{\sigma_1}\right|^{\frac{2}{n}} - \left|\frac{u_2}{\sigma_2}\right|^{\frac{2}{n}}\right); \quad n \neq 1, \quad (12)$$

where the parameters $\sigma_i; i = 1, 2$ are anisotropic correlation lengths in each direction. Equation (12) for $n = 1$ is reduced to an elliptical form which is considered in the previous subsection. Hence, Eq. (12) is different from the exponential kernel function of the form $k(r) = \sigma^2 \exp\left[-\left(\frac{r}{\sigma}\right)^v\right]$ that is considered by Abrahamsen (1997). Different forms of super-ellipsoid functions for some values of the isolevel contours n are plotted in Fig. 2. The contours are rounded rectangles for $n < 1$, ellipses for $n = 1$, concave diamonds for $1 < n < 2$, diamonds for $n = 2$, and convex diamonds for $n > 2$.

Substituting (12) into (1), we obtain a new anisotropic covariance function of the form
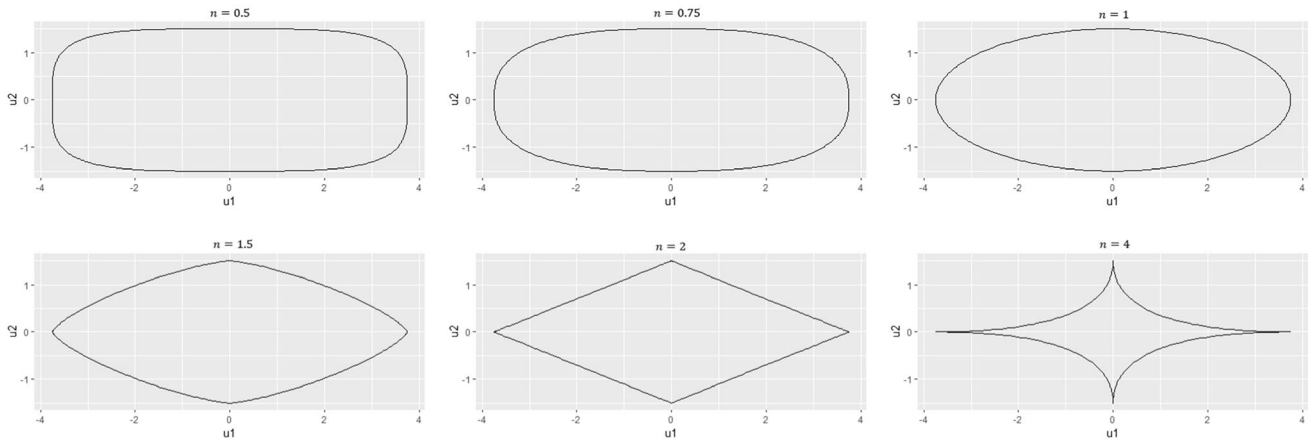
$$C(x, y) = \int_{\mathbb{R}^2} \sigma^4 \exp\left(-\left|\frac{x_1 - v_1}{\sigma_1}\right|^{\frac{2}{n}} - \left|\frac{x_2 - v_2}{\sigma_2}\right|^{\frac{2}{n}} \right. \\ \left. -\left|\frac{y_1 - v_1}{\sigma_1}\right|^{\frac{2}{n}} - \left|\frac{y_2 - v_2}{\sigma_2}\right|^{\frac{2}{n}}\right)dv, \quad (13)$$

where $v = (v_1, v_2) \in \mathbb{R}^2$. It is hard to obtain a close form for (13). The super-ellipsoidal kernel function defined in (12) is not elliptic because it does not satisfy the relation in $C(u) = C_0(u\Sigma^{-1}u^t), u \in \mathbb{R}^2$ where u is the separation vector of x and y, Σ is a 2×2 symmetric and positive-definite matrix with positive determinant, and $C_0 : \mathbb{R} \to [0, \infty)$ is a Borel function (Møller and Toftaker 2014). Thus, the covariance function constructed in terms of auto-convolution of super-ellipse functions is not elliptic and so it is not reducible to an isotropic case under a rotation, except for the case $n = 1$, for which we get back the ellipsoidal covariance function. We thus provide a new class of LGCPs models in terms of non-elliptical anisotropic covariance functions.

Now, consider X as a LGCP driven by intensity function $\Lambda(x) = \exp\{Z(x)\}$, where $Z(x)$ is a zero mean Gaussian random field with variance σ^2 and covariance function $C(.)$ defined in (13). Similar to the previous Gaussian LGCP model in Example 1, the pair correlation function and K-function over a bounded set $A = C(0, \rho)$ can be obtained using (4), (7) and (13), respectively,

$$g(x, y) = \exp\left\{\int_{\mathbb{R}^2} \sigma^4 \exp\left(-\left|\frac{x_1 - v_1}{\sigma_1}\right|^{\frac{2}{n}} - \left|\frac{x_2 - v_2}{\sigma_2}\right|^{\frac{2}{n}}\right.\right. \\ \left.\left. -\left|\frac{y_1 - v_1}{\sigma_1}\right|^{\frac{2}{n}} - \left|\frac{y_2 - v_2}{\sigma_2}\right|^{\frac{2}{n}}\right)dv\right\}, \quad (14)$$

and

Fig. 2 Isolevel contours of the super-ellipsoid functions for different values of the index $n = 0.5, 0.75, 1, 1.5, 2, 4$

$$K(\rho) = \int_{\|u\| \leq \rho} g(u)du, \tag{15}$$

where $g(u)$ is defined in (14) and u is the separation vector of x and y. Section 3.2 studies in detail the LGCP in terms of the exponential super-ellipsoidal covariance function and its corresponding pair correlation and K-functions.

3.1.2 Method 2: Normal variance mixture covariance functions

Consider $p(X; s)$ a probability density function for X, parameterized by s such that for each value of s in some set A, $p(X; s)$ is a probability density function with respect to X. Given a probability density function ω, which is non-negative and integrates to 1, the function

$$f(x) = \int_A p(X; s)\omega(s)ds, \tag{16}$$

is again a probability density function for X. Jalilian et al. (2013) introduced a new class of isotropic shot noise Cox processes in which both the kernel function and the pair correlation function are given based on a normal variance mixture. Modeling the shape at the origin and the tail behavior of the pair correlation function can be easier and more flexible when using the normal variance mixture. We now follow a similar procedure as in Sect. 3.1.1 to obtain a new anisotropic class of LGCPs based on normal variance mixtures. It is worth recalling that the normal variance mixture is defined by

$$f(u) = \int_0^\infty \Phi(u; s)h(s)ds, \tag{17}$$

where $\Phi(.; s)$ is the density of a zero-mean two-dimensional anisotropic Gaussian vector with covariance matrix sM, $M = diag(\sigma_1, \sigma_2)$, and h is some prior probability density of s on $\mathbb{R}^+$. Any function f defined as in (17) is a

positive definite function on $\mathbb{R}^2$ (Schlather 1999). By a similar argument to the isotropic case, if h is a convolution of a function $\tilde{h}$ with itself, i.e. $h = \tilde{h} * \tilde{h}$, then f is the convolution of a non-negative function k with itself, $f = k * k$, where the function k is defined by

$$k(u) = \int_0^\infty \Phi(u; s)\tilde{h}(s)ds. \tag{18}$$

According to the relation between Eqs. (17) and (18), f can be considered a covariance function. Thus, there is no need, as in Sect. 3.1.1, to consider a kernel function and to define the covariance as a convolution of kernels. We can directly use (17). A huge class of covariance functions are obtained by choosing h in the class of generalized inverse Gaussian distributions (Jørgensen, 2012) which includes Gamma, inverse Gamma and inverse Gaussian distributions as special cases. The resulting class of normal variance mixtures is the class of generalized hyperbolic distributions (Barndorff-Nielsen 1977, 1978). Following Barndorff-Nielsen and Halgreen (1977), any generalized inverse Gaussian distribution is infinitely divisible, and hence any generalized hyperbolic density can be represented as a convolution. However, for a generalized inverse Gaussian density h, it is not always easy to identify the convolution density $\tilde{h}$. We discuss below two special cases of generalized hyperbolic distributions where $\tilde{h}$, and hence k, are explicitly known and we can obtain the generalized Cauchy covariance function. The Cauchy covariance function is polynomially decreasing, and hence more suitable than the Matérn model for modeling slowly decaying covariances. The Cauchy covariance is log-concave in a neighborhood around the origin.

Example 3 Cauchy covariance model

Assume that s in (18) is a random variable with an inverse Gamma density with parameters $\alpha, \beta > 0$ of the form

$$h(s; \alpha, \beta) = \beta^\alpha s^{-\alpha-1} \exp\{-\beta/s\}/\Gamma(\alpha), s > 0. \tag{19}$$

Let $\alpha = 1/2$. It can be shown that $h(\cdot; 1/2, \beta)$ is a convolution of $h(\cdot; 1/2, \beta/4)$ with itself.

Following (17) and (18), a covariance function can be defined through a normal variance mixture with the function $h(\cdot; 1/2, \beta)$, as follows

$$C(u) = \int_0^\infty \frac{1}{2\pi s\sqrt{\sigma_1\sigma_2}} \exp\left\{-\frac{u_1^2}{2\sigma_1 s} - \frac{u_2^2}{2\sigma_2 s}\right\}$$

$$\frac{\beta^{\frac{1}{2}}}{\Gamma\left(\frac{1}{2}\right)} s^{-\frac{3}{2}} \exp\{-\beta/s\} ds$$

$$= \frac{\beta^{\frac{1}{2}}}{2\pi\sqrt{\pi\sigma_1\sigma_2}} \int_0^\infty s^{-\frac{5}{2}} \exp\{-\beta^*/s\} ds$$

$$= \frac{\beta^{\frac{1}{2}}}{\beta^{*\frac{3}{2}} 4\pi\sqrt{\sigma_1\sigma_2}},$$

where $\beta^* = \frac{2\beta\sigma_1\sigma_2 + \sigma_2 u_1^2 + \sigma_1 u_2^2}{2\sigma_1\sigma_2}$. This expression can be rewritten as an anisotropic generalized Cauchy function

$$C_{aniso}(u) = \frac{1}{4\pi\beta\sqrt{\sigma_1\sigma_2}} \left[1 + \frac{u_1^2}{2\sigma_1\beta} + \frac{u_2^2}{2\sigma_2\beta}\right]^{-\frac{3}{2}}, \tag{20}$$

with anisotropic parameters $\sigma_1^* = \sigma_1\beta$, and $\sigma_2^* = \sigma_2\beta$.

Equivalently,

$$C_{aniso}(u) = \sigma^2[1 + u^\tau \Sigma^{-1} u]^{-\frac{3}{2}},$$

where $\sigma^2 = \frac{1}{4\pi\sqrt{\sigma_1^*\sigma_2^*}}$ is the variance and Σ is an anisotropic diagonal matrix with elements $(2\sigma_1^*, 2\sigma_2^*)$. Clearly, this anisotropic covariance function can be written in terms of the isotropic function, that is,

$$C_{aniso}(u) = C_{iso}(u^\tau \Sigma^{-1} u),$$

where $C_{iso}(\cdot)$ is an isotropic Cauchy covariance function defined by $C_{iso}(v) = \sigma^2[1 + v]^{-\frac{3}{2}}$. As mentioned in Sect. 3.1.1, the pair correlation function and the covariance function are exponentially linked in LGCPs. Therefore, the pair correlation function can be obtained as

$$g_{aniso}(u) = \exp\left\{\frac{1}{4\pi\sqrt{\sigma_1^*\sigma_2^*}}[1 + \frac{u_1^2}{2\sigma_1^*} + \frac{u_2^2}{2\sigma_2^*}]^{-\frac{3}{2}}\right\}$$

$$= \exp\left\{\sigma^2[1 + u^\tau \Sigma^{-1} u]^{-\frac{3}{2}}\right\}. \tag{21}$$

Again, we note that, $g_{aniso}(u) = g_{iso}(u^\tau \Sigma^{-1} u)$ where $g_{iso}(\cdot)$ is an isotropic Cauchy pair correlation function defined by $g_{iso}(v) = exp\left\{\sigma^2[1 + v]^{-\frac{3}{2}}\right\}$.

Substituting (21) into (7), the anisotropic K-function

over the disc $A = C(0, \rho)$, denoted by K_{aniso}^C, is given by

$$K_{aniso}^C(\rho) = \int_{\|u\| \leq \rho} \exp\left\{\frac{1}{4\pi\sqrt{\sigma_1^*\sigma_2^*}}[1 + \frac{u_1^2}{2\sigma_1^*} + \frac{u_2^2}{2\sigma_2^*}]^{-\frac{3}{2}}\right\} du.$$

Example 4 Generalized Cauchy covariance model

Consider now that s follows a Gamma density

$$h(s; \alpha, \beta) = \beta^\alpha s^{\alpha-1} \exp\{-\beta s\}/\Gamma(\alpha), \ s > 0, \tag{22}$$

with parameters $\alpha, \beta > 0$ which is a convolution of $h(\cdot; \alpha/2, \beta)$ with itself. The corresponding covariance function is then obtained as

$$C(u) = \int_0^\infty \frac{s}{2\pi\sqrt{\sigma_1\sigma_2}} \exp\left\{-\frac{su_1^2}{2\sigma_1} - \frac{su_2^2}{2\sigma_2}\right\}$$

$$\frac{\beta^\alpha}{\Gamma(\alpha)} s^{\alpha-1} \exp\{-\beta s\} ds$$

$$= \frac{\beta^\alpha}{2\pi\sqrt{\sigma_1\sigma_2}\Gamma(\alpha)} \cdot \frac{\Gamma(\alpha+1)}{(\beta^*)^{\alpha+1}},$$

where $\beta^* = \beta + \frac{u_1^2}{2\sigma_1} + \frac{u_2^2}{2\sigma_2}$. We can rewrite it as an anisotropic generalized Cauchy function

$$C_{aniso}(u) = \frac{\alpha}{2\pi\beta\sqrt{\sigma_1\sigma_2}} \left[1 + \frac{u_1^2}{2\sigma_1\beta} + \frac{u_2^2}{2\sigma_2\beta}\right]^{-(\alpha+1)}, \tag{23}$$

with anisotropic parameters $\sigma_1^* = \sigma_1\beta$, and $\sigma_2^* = \sigma_2\beta$.

Equivalently,

$$C_{aniso}(u) = \sigma^2[1 + u^\tau \Sigma^{-1} u]^{-(\alpha+1)},$$

where $\sigma^2 = \frac{\alpha}{2\pi\sqrt{\sigma_1^*\sigma_2^*}}$ is the variance and Σ is an anisotropic diagonal matrix with elements $(2\sigma_1^*, 2\sigma_2^*)$. So

$$C_{aniso}(u) = C_{iso}(u^\tau \Sigma^{-1} u),$$

where $C_{iso}(\cdot)$ is an isotropic Cauchy covariance function defined by $C_{iso}(v) = \sigma^2[1 + v]^{-(\alpha+1)}$.

According to (4), the pair correlation function of a LGCP model can be obtained as

$$g_{aniso}(u) = \frac{\alpha}{2\pi\sqrt{\sigma_1^*\sigma_2^*}}[1 + \frac{u_1^2}{2\sigma_1^*} + \frac{u_2^2}{2\sigma_2^*}]^{-(\alpha+1)}, \tag{24}$$

or equivalently,

$$g_{aniso}(u) = \exp\left\{\sigma^2[1 + u^\tau \Sigma^{-1} u]^{-(\alpha+1)}\right\}.$$

Here, $g_{aniso}(u) = g_{iso}(u^\tau \Sigma^{-1} u)$ where $g_{iso}(\cdot)$ is an isotropic Cauchy pair correlation function defined by $g_{iso}(v) = \exp\left\{\sigma^2[1 + v]^{-(\alpha+1)}\right\}$.

Using (24) and (7), the anisotropic K-function over the disc $A = C(0, \rho)$, denoted by K_{aniso}^{GC}, is given by

$$K_{aniso}^{GC}(\rho) = \int_{\|u\| \le \rho} \frac{\alpha}{2\pi\sqrt{\sigma_1^*\sigma_2^*}}[1 + \frac{u_1^2}{2\sigma_1^*} + \frac{u_2^2}{2\sigma_2^*}]^{-(\alpha+1)}du.$$

3.2 Non-elliptical and anisotropic exponential super-ellipse covariance model

Let X be a LGCP driven by an anisotropic intensity function $\Lambda(x) = \exp\{Z(x)\}$, where $Z(x)$ is a zero-mean Gaussian random field with variance σ^2 and an anisotropic covariance function $C(.)$. We are interested in building our new anisotropic LGCP model based on an anisotropic exponential super-ellipsoidal covariance function defined in (12), where $u = (u_1, u_2)$ is the separation vector and σ_i, $i = 1, 2$ are anisotropic covariance parameters in each direction that are turned separately. Substituting (12) into (4), we can obtain a close analytic form for the anisotropic pair correlation function, given by

$$g(u) = \exp\left\{\sigma^2 \exp\left\{-\left|\frac{u_1}{\sigma_1}\right|^{\frac{2}{n}} - \left|\frac{u_2}{\sigma_2}\right|^{\frac{2}{n}}\right\}\right\}. \tag{25}$$

Consider a bounded set $A = C(o, \rho)$, and substituting (25) into (7) we can obtain the K-function of our new model over a disc A, denoted by $K^{ESE}(.)$, as

$$K^{ESE}(\rho) = \int_{\|u\| \le \rho} \exp\left\{\sigma^2 \exp\left\{-\left|\frac{u_1}{\sigma_1}\right|^{\frac{2}{n}} - \left|\frac{u_2}{\sigma_2}\right|^{\frac{2}{n}}\right\}\right\}du. \tag{26}$$

4 A moment-based estimation method

Let $\mathbb{S}$ denote a bounded window in $\mathbb{R}^2$. Suppose that X is a LGCP model defined on $\mathbb{S}$, driven by the random intensity function $\Lambda(x) = \exp\{\gamma + Z(x)\}$, where $Z(x)$ is a Gaussian process with anisotropic covariance parameters σ_1 and σ_2. A parameter estimation procedure for these anisotropic LGCP models is presented in this section. Let $\lambda(.)$ be the intensity of X, a realization of the random intensity Λ. A non-parametric kernel estimation method is often used to estimate the intensity function of a realization of $X = \{x_i\}_{i=1}^n$, and is given by

$$\widehat{\lambda}(u) = \sum_{i=1}^n k(u - x_i)/e(x_i), \tag{27}$$

for any location point $u \subseteq \mathbb{S}$, where $k(u)$ is the kernel function and $e(u) = \int k(u - v)dv$ is an edge correction (Diggle 1985; Baddeley et al. 2015). For parameter estimation, we consider the least squares estimation method that is a moment-based estimation technique based, in our case, on minimizing a measure of the difference between a

theoretical K-function and an empirical one. Note that a moment-based estimation method can be also constructed in terms of the pair correlation function, but it is preferred to consider the K-function rather than the pair correlation function (Møller and Toftaker 2014). This procedure based on g-function depends on the kernel estimator $\hat{g}$, and so a suitable choice of the bandwidth in the kernel defined in $\hat{g}$ is clearly necessary. Using the K-function, we avoid kernel estimation.

We also note that there are alternative several inferential methods we can follow to estimate the parameters of our models, such as likelihood-based estimation or Bayesian estimation. For models as the ones we have with parameters providing information on anisotropy, the likelihood provides several possible local maximum estimates, and its convergence can be very slow and can not even converge. In these cases, the moment-based estimators are more robust. We are not following the Bayesian approach as our models are shown to have a close form of the summary statistics that we can work with, and thus there is no need to be helped by MCMC simulations of a posterior distribution. We thus follow moment-based estimation and show that this is a convenient and useful method of estimation for our anisotropic models.

Assume that the model incorporates a vector of unknown parameters θ. Let K_T and K_E denote the theoretical and the empirical K-functions, respectively. A discrepancy criterion to measure the difference between the model, determined by K_T, and empirical data, determined by K_E, is given by

$$D(\theta) = \int_0^{\rho_0} w(\rho)\{K_T(\rho, \theta)^c - K_E(\rho)^c\}^2 d\rho, \tag{28}$$

where the constant ρ_0, the power transformation c, and the weighting function $w(\rho)$ are to be chosen. The value $\widehat{\theta}$ obtained by minimizing (28) is considered the estimated value of the vector of unknown parameters θ. It is difficult to give a general rule to choose the values ρ_0 and c. Expression (28) is sensitive to ρ_0, and it should not be too large (Diggle 2013). For data on a rectangular region with side-lengths a and b, the value of ρ_0 has to be larger than $0.25 \times min(a, b)$. The function $rmax.rule(.)$ in the $spatstat$ package helps to calculate this value. The values of c and $w(\rho)$ are related to the sampling fluctuations of the empirical K-function $K_E(\rho)$. These fluctuations increase with ρ and so have direct influence on $\widehat{\theta}$. Diggle (2013) described how to choose ρ_0 and c and suggested that, by empirical experience with real and simulated data, $c = 0.5$ and $w(\rho) = 1$ is a reasonable choice when fitting a model to regular patterns. However, for aggregated patterns $c = 0.25$ is usually more effective. The variance of $\sqrt{\widehat{K}(\rho)}$ in

Poisson processes does approximately not depend on ρ, so for patterns which are not far different from complete spatial randomness, $c = 0.5$ is a good choice which acts as a variance-stabilizing transformation (Besag 1977; Diggle 2013). In the general case, an inhomogeneous reduced second moment measure for any bounded set A in $\mathbb{R}^2$ can be estimated by

$$\kappa_E(A) = \sum_{\substack{x_i, x_j \in \mathbb{S} \\ (x_i \neq x_j)}} \frac{I_A(x_j - x_i)}{\widehat{\lambda}(x_i)\widehat{\lambda}(x_j)} e(x_i, x_j), \tag{29}$$

where $\mathbb{S}$ is a rectangular window with side-lengths a and b, I stands for the indicator function that indicates if the distance between points x_i and x_j lies in A, and $e(x_i, x_j)$ is a weighting function that corrects for edge effects. This weighting function is defined by $\frac{1}{v(\mathbb{S} \cap \mathbb{S}_{x_j - x_i})}$ for the pairs of points (x_i, x_j), where $v(\mathbb{S} \cap \mathbb{S}_z)$, represents a measure of the intersection of the set $\mathbb{S}$ with the translated set $\mathbb{S}_z$, which is the result of shifting the window $\mathbb{S}$ by the vector z. For a rectangular set $\mathbb{S}$, $e(x_i, x_j)$ is the Ohser and Stoyan's translation edge correction, and in this case $v(\mathbb{S} \cap \mathbb{S}_z) = \frac{(a - \|\xi\|)(b - \|\eta\|)}{ab}$, where $z = (\xi, \eta)$ (Illian et al. 2008). The function *edge.Trans(.)* in package *spatstat* computes Ohser and Stoyan's translation edge correction weights for a point pattern (Ohser 1983). Following Baddeley (1999) and Illian et al. (2008), it can be proved that $\kappa_E(A)$ is an unbiased estimator of $\kappa_T(A)$.

As an illustration of the validity of the least square method, we present two cases, one elliptical and another one a non-elliptical example. For an elliptical model, consider an inhomogeneous and anisotropic two-dimensional LGCP with a Gaussian covariance function as in Eq. (3). Assume $\sigma_1 = 0.05$, and $\sigma_2 = 0.8$. Consider the function $\lambda(x) = \exp\{\gamma + Z(x)\}$ for the intensity function, with Z a Gaussian random field. Here, we have fixed $\gamma = 5$. As a second illustration for a non-elliptical model, consider an inhomogeneous and anisotropic two-dimensional LGCP with a non-elliptical exponential super-ellipse covariance function as in Sect. 3.2. Assume $\sigma_1 = 0.04$, $\sigma_2 = 0.2$ and $\sigma^2 = 1$. Consider the function $\lambda(x) = \exp\{\gamma + Z(x)\}$ for the intensity function, with Z a Gaussian random field with an exponential super-ellipse covariance function.

Our goal is to estimate the (usually unknown) values of the anisotropic covariance parameters σ_1 and σ_2. We make use here, and in the next sections, of the R packages *RandomFields* (Schlather et al. 2015), *spatstat* (Baddeley and Turner 2005), *fields*, *mvtnorm* and *plotly*. In these packages, we can find all the necessary functions that we have used for simulation, model fitting and model validation of our models.

We first simulated a zero mean Gaussian random field $Z(\cdot)$ with a Gaussian covariance function as in Eq. (3) on the unit square $\mathbb{S} = [0, 1] \times [0, 1]$, as shown as a pixel image in Fig. 3 (top left). We then obtained the intensity function $\lambda(\cdot)$, as a realization of the simulated random field. This intensity is shown as an image in Fig. 3 (top right). Based on this intensity image, we simulated a realization of an inhomogeneous Poisson point process with 286 events, as shown in Fig. 3 (bottom left). Finally, we estimated the anisotropic parameters. We used (8) as the theoretical K-function over a disc A, and (29) as the corresponding empirical estimator for the least square function $D(\theta)$ in (28), where A denotes a disc centered at the origin with radius ρ. Figure 3 (bottom right) shows the least square function $D(\theta)$ with respect to different values of σ_1 and σ_2. We note that this function has a minimum, and its minimization provides $\widehat{\sigma}_1 = 0.04381$ and $\widehat{\sigma}_2 = 0.83741$, values that are certainly close to the initial ones, providing a graphical and simple indication that the least square method presented in (28) works for parameter estimation.

For second non-elliptical example, we first simulated a zero mean Gaussian random field $Z(\cdot)$ with an exponential super-ellipse covariance function as in Eq. (12), as described in Sect. 3.2, on the unit square $\mathbb{S} = [0, 1] \times [0, 1]$, as shown as a pixel image in Fig. 4 (top left). Then, we obtained the corresponding intensity function which is shown as an image in Fig. 4 (top right). In terms of this intensity pixel image, we simulated a realization of an inhomogeneous LGCP with 243 events, as shown in Fig. 4 (bottom left). Finally, as described above, we used the least square function defined in (28) to proceed with the estimation of the anisotropic parameters, where (26) was considered as the theoretical K-function, and (29) as the corresponding empirical K-function. The least square function $D(\theta)$ with respect to different values of σ_1 and σ_2 is shown in Fig. 4 (bottom right) which shows a minimum value at $\widehat{\sigma}_1 = 0.04216$ and $\widehat{\sigma}_2 = 0.19973$; both are quite close to the true values, and again confirms that the least square method works well for parameter estimation.

5 Simulation experiments

We carried out a simulation study for a number of scenarios to investigate the performance of our estimation procedure. We assume to work on the unit square, $\mathbb{S} = [0, 1] \times [0, 1] \subseteq \mathbb{R}^2$. For each LGCP model described in Sect. 3, we simulated 200 realizations for known values of the anisotropic parameters, and estimated them using our proposed moment-based method as presented in Sect. 4. We additionally checked the goodness-of-fit of our four LGCP models.
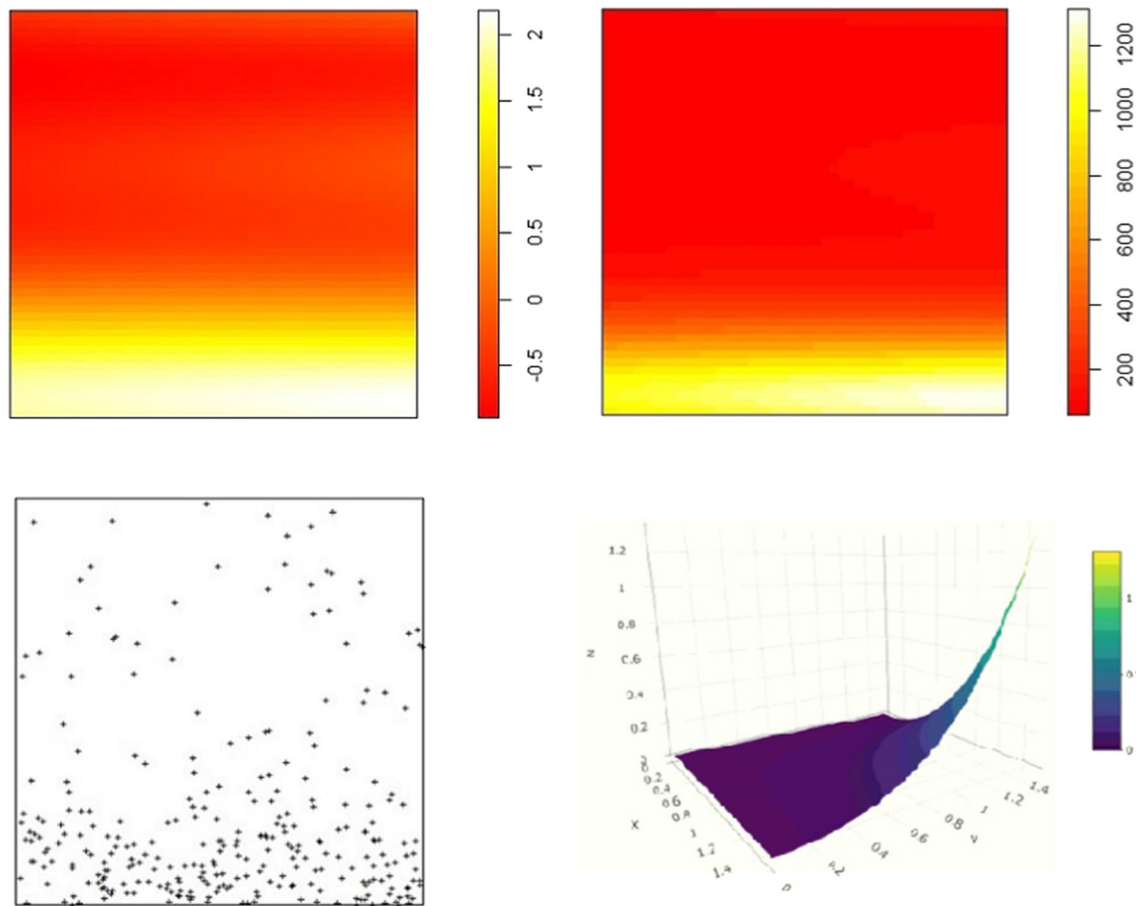
Fig. 3 *Top left*: Simulated random field with a Gaussian covariance function as in Eq. (3) on the unit square $\mathbb{S} = [0, 1] \times [0, 1]$. *Top right*: Intensity image as a realization coming from the exponential of the random field. *Bottom left*: A realization of the inhomogeneous Poisson process giving rise to an anisotropic LGCP with 286 points. *Bottom right*: The least square function

We first considered 200 realizations from the anisotropic LGCP in Example 1 of Sect. 3.1.1, based on the anisotropic Gaussian covariance function in Eq. (3), with scale parameters given by $\sigma_1 = 0.05$ and $\sigma_2 = 0.8$. We refer to this case as *Model 1*. Figure 5, row 1, represents a simulation of the corresponding underlying random field $Z(\cdot)$ with covariance function given in (3), together with the intensity $\Lambda(x) = \exp\{\gamma + Z(x)\}$, with a fixed value $\gamma = 5$ and a realization with 286 points of the anisotropic LGCP for *Model 1*.

As a second scenario, we considered 200 realizations from the anisotropic LGCP in Example 3 of Sect. 3.1.2, based on the anisotropic generalized Cauchy covariance function defined in Eq. (20), with anisotropic parameters given by $\sigma_1 = 0.2$ and $\sigma_2 = 0.045$, and with the scale parameter of the Cauchy covariance $\beta = 1$. We refer to this case as *Model 2*. Figure 5, row 2, represents a simulation of the corresponding underlying random field $Z(\cdot)$ with covariance function given in (20), together with the intensity $\Lambda(x) = \exp\{\gamma + Z(x)\}$ with $\gamma = 6$ and a realization with 265 points of the anisotropic LGCP for *Model 2*.

As a third scenario, we considered 200 realizations from the anisotropic LGCP in Example 4 of Sect. 3.1.2, based on the anisotropic generalized Cauchy covariance function defined in Eq. (23), with anisotropic parameters given

by $\sigma_1 = 3.5$ and $\sigma_2 = 1.7$, and with the scale parameters of the Cauchy covariance $\alpha = 2$ and $\beta = 1$. We refer to this case as *Model 3*. Figure 5, row 3, represents a simulation of the corresponding underlying random field $Z(\cdot)$ with covariance function given in (23), together with the intensity $\Lambda(x) = \exp\{6 + Z(x)\}$ and a realization with 442 points of the anisotropic LGCP for *Model 3*.

Finally, and for a fourth scenario, we considered 200 realizations from the non-elliptical and anisotropic LGCP described in Sect. 3.2, based on the anisotropic exponential super-ellipse covariance function in (12), with anisotropic parameters given by $\sigma_1 = 4$ and $\sigma_2 = 2$, and variance $\sigma_x^2 = 1$. We refer to this case as *Model 4*. Figure 5, row 4, represents a simulation of the corresponding underlying random field $Z(\cdot)$ with covariance function given in (12), together with the intensity $\Lambda(x) = \exp\{\gamma + Z(x)\}$ with $\gamma =$
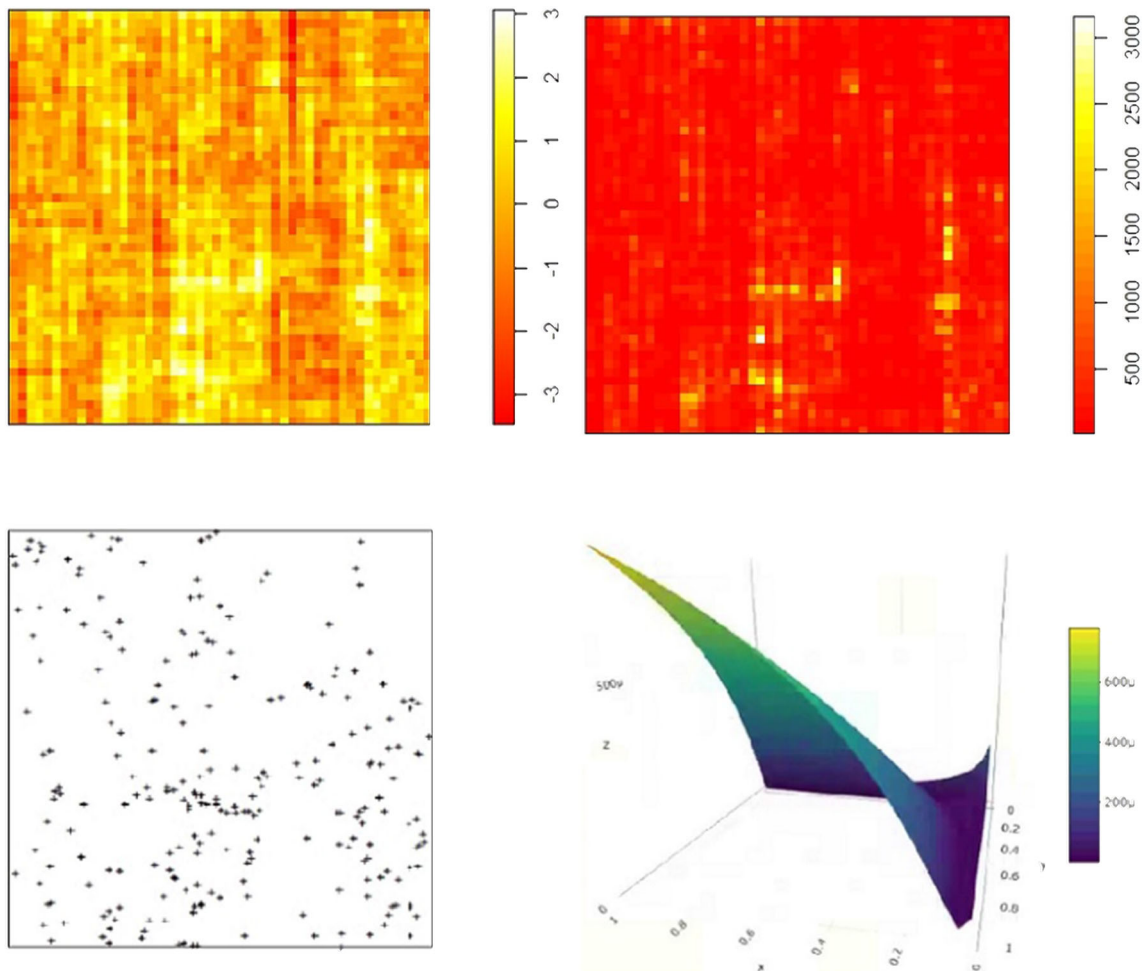
Fig. 4 *Top left*: Simulated random field with an exponential super-ellipse covariance function as in Eq. (12) on the unit square $\mathbb{S} = [0, 1] \times [0, 1]$. *Top right*: Intensity image as a realization of the exponential of the random field. *Bottom left*: A realization of the inhomogeneous Poisson process giving rise to an anisotropic LGCP with 243 points. *Bottom right*: The least square function

5 and a realization with 188 points of the anisotropic LGCP for *Model 4*.

Models 1–4 in Fig. 5 should show some sort of anisotropy. For a simple assessment of anisotropy, we follow Baddeley et al. (2015) that suggested to compare the sector K-function for two 30° sectors centred on the x and y axes, i.e., the angle between $-15°$ and $15°$ and the angle between $90 - 15°$ and $90 + 15°$, measured anticlockwise from the x-axis. Anisotropy would be suggested if these two functions were unequal. Figure 6 shows the sector K-functions for 30° sectors centred on the horizontal and vertical axis for the particular realization chosen in Fig. 5 for each one of *Models 1–4*. Anisotropy is clear in all cases, in particular in *Models 1,2*, for which the two sector K-functions are certainly different.

Our simulations come from models for which we know the theoretical analytical form. We thus, as an additional assessment, compare the empirical K-function coming from the simulated patterns with the theoretical anisotropic K-function. We also consider the K-function under a Poisson process over a disc centered at the origin with radius ρ, whose form is $K^{Pois}(\rho) = \pi\rho^2$ (see Fig. 7).

It is clearly noted that all four models reflect a clustering behavior as the K-functions are all above the Poisson function, and, as expected, the empirical and theoretical K-functions behave in a similar way far from the random case, represented by the Poisson functions. This is a direct consequence of the structure imposed by a LGCP with a varying intensity depending on a random field with a particular correlation structure. The implication of clustering is that the conditional intensity of cases at an arbitrary location y, given a case at a nearby location x, is greater than the unconditional intensity of cases at y, i.e., clustering involves a form of dependence between cases.

Finally, we estimated all parameters of the four models for each one of the 200 realizations. The results in form of point estimations, mean absolute percentage error (MAPE),
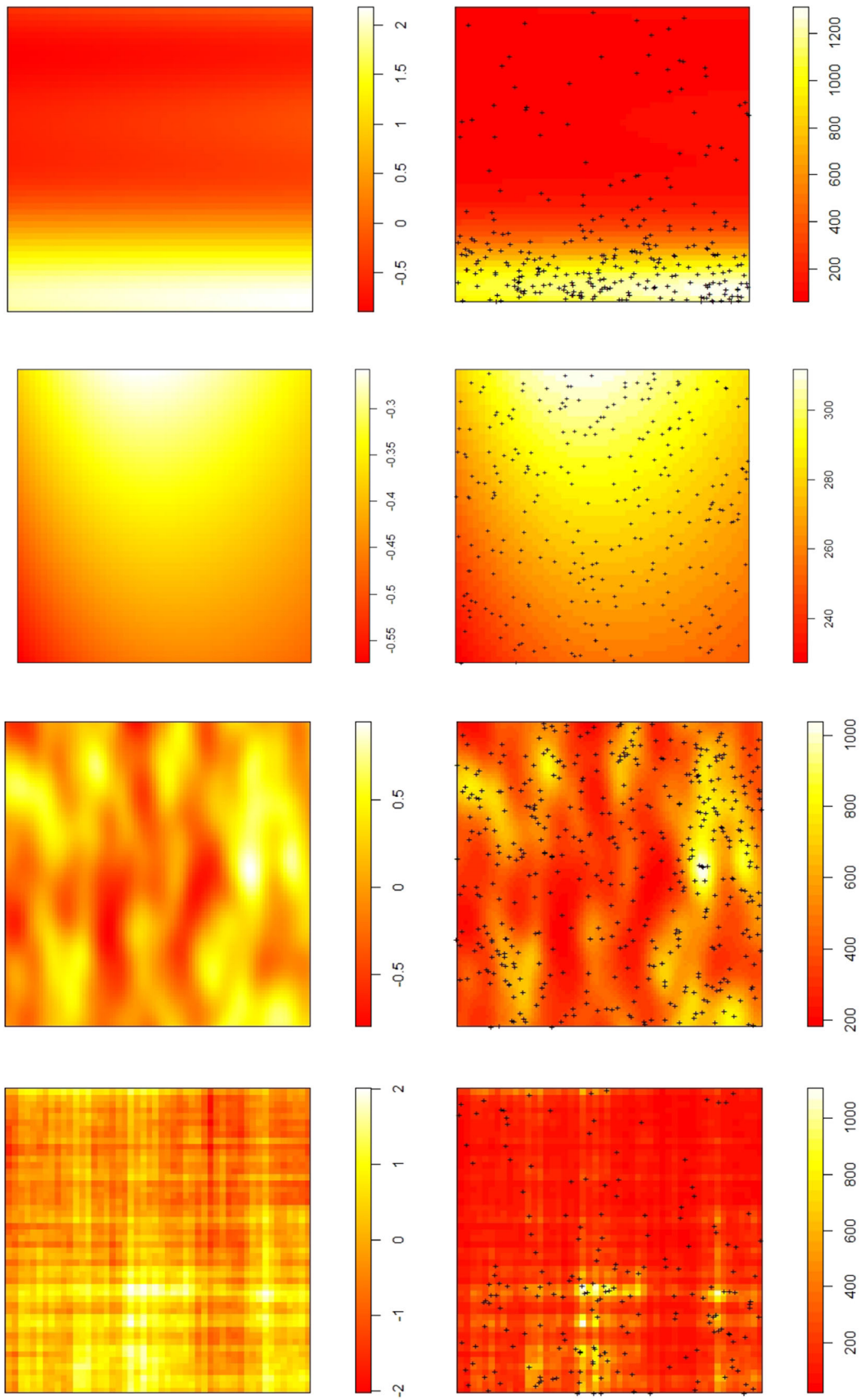
◄**Fig. 5** Representations of the random fields (*First column*), and of intensities and point pattern realizations of the anisotropic LGCP (*Second column*) for each one of the four models considered (each row represents Model 1 up to Model 4). *Row 1*: Random field $Z(\cdot)$ with covariance function as in (3), and intensity $\Lambda(x) = \exp\{5 + Z(x)\}$ together with a realization of the inhomogeneous Poisson process, for *Model 1*. *Row 2*: Random field $Z(\cdot)$ with covariance function as in (20), and intensity $\Lambda(x) = \exp\{\gamma + Z(x)\}$, with a fixed value $\gamma = 6$, together with a realization of the inhomogeneous Poisson process, for *Model 2*. *Row 3*: Random field $Z(\cdot)$ with covariance function as in (23), and intensity $\Lambda(x) = \exp\{6 + Z(x)\}$, together with a realization of the inhomogeneous Poisson process, for *Model 3*. *Row 4*: Random field $Z(\cdot)$ with covariance function as in (12), and intensity $\Lambda(x) = \exp\{5 + Z(x)\}$, together with a realization of the inhomogeneous Poisson process, for *Model 4*

mean squared error (MSE), standard deviations (SD), and confidence intervals (CI) are shown in Table 1.

We note that the estimations are close to the theoretical values of the parameters, and the corresponding MAPE, MSE and SD values are certainly small. Also, the true values of the parameters θ are well inside the 95% confidenceintervals, given by $\widehat{\theta} \pm 1.96 SD\left(\widehat{\theta}\right)$, where θ stands for any particular parameter $(\alpha, \sigma_1, \sigma_2, \sigma^2)$.These results are reinforced by graphical outputs in terms of histograms and boxplots (see Figs. 8 and 9). The true parameters are clearly lying inside the distribution of the estimated parameters. Only in one case, we find a small number of outliers, but even for this case, the difference with respect to the mean is so small that they have no particular effect. Also, Fig. 10 shows the theoretical K-function based on the true values of parameters and the theoretical K-functions coming from the estimated values for each model. In all cases, the theoretical K-function based on the true values are well inside the theoretical K-functions coming from the estimated parameters, which is an indication of robust behavior of the estimation procedure.

We note that the moment-based estimator based on a minimum contrast method provides a reasonable performance for all mentioned models. The estimation for all parameters are close to the theoretical ones with a small variation in all cases. They show some symmetry and there are hardly outlying estimates. The procedure works equally fine for all the new theoretical models.

6 Application: analysis of earthquake datasets

Earthquakes are the most unpredictable and devastating natural disasters which are usually caused when rock underground suddenly breaks along a fault. This releases a sudden energy that causes the seismic waves making the ground shake. When high-intensity earthquakes strike, they can cause massive devastation, thousands of deaths, and lots of economical losses in damaged properties. The level of damages mainly depends on the earthquake magnitude and depth.

We have considered two datasets of earthquakes, one in South America and the other in the Mediterranean Europe, see Fig. 11. The datasets include the occurrence times, magnitudes, longitude, latitude, and depth. In particular, we focussed on the epicenters of those earthquakes with magnitude equal or larger than 4 occurred between January 1950 and June 1998.

6.1 Analysis of earthquakes in South America

We considered earthquake events with magnitude equal or larger than 4 occurred between January 1950 and June 1998 in South America within a rectangular region of latitude between $-58S$ and $18N$, and longitude between $-80W$ and $-40E$. The dataset contains 586 earthquakes, as shown in Fig. 12.

We first assessed the condition of anisotropy as described in Sect. 5. Figure 13 shows the corresponding sector K-functions for $30°$ sectors centred on the horizontal and vertical axis for the South America earthquake events. We see that both sector K-functions are clearly different indicating an anisotropic behavior.

We estimated the intensity function by the non-parametric kernel estimator given by (27). This estimated intensity is plugged into the empirical estimator of the K-function (see Eq. (29)). Although we fitted all models (*Models 1–4*), we only report the results of *Models 1,4*, as the other two were not providing a good fit. We thus fittedthe elliptic anisotropic LGCP based on the anisotropic Gaussian covariance function in (3) (*Model 1*), and the non-elliptic anisotropic LGCP based on the anisotropic exponential super-ellipse covariance function in (12) (*Model 4*), respectively. We used the least square method given in (28) to estimate the anisotropic parameters. Optimization of the least square function resulted in the following estimates: $\hat{\sigma}_1 = 0.15232$ and $\hat{\sigma}_2 = 0.03307$ for *Model 1*, and $\hat{\sigma}_1 = 0.35145$, $\hat{\sigma}_2 = 1.254$ and $\sigma^2 = 1.0124$ for *Model 4*.

We highlight the clustering behavior of the earthquakes indicated by the fact that the empirical K-function estimated from the events is far from (and on top of) the K-function under a Poisson process, as shown in Fig. 14.

Finally, to formally assess the goodness-of-fit of *Models 1,4* to the earthquake events, we simulated 39 point patterns with the estimated parameters coming from the fit of both models. We calculated the envelopes from the

Fig. 6 Assessment of anisotropy using sector *K*-functions for the realizations in Fig. 5. *First column*: Sector *K*-functions for 30° sectors centred on the horizontal axis. *Second column*: Sector *K*-functions for 30° sectors centred on the vertical axis. Each row corresponds to each one of the four considered models, respectively
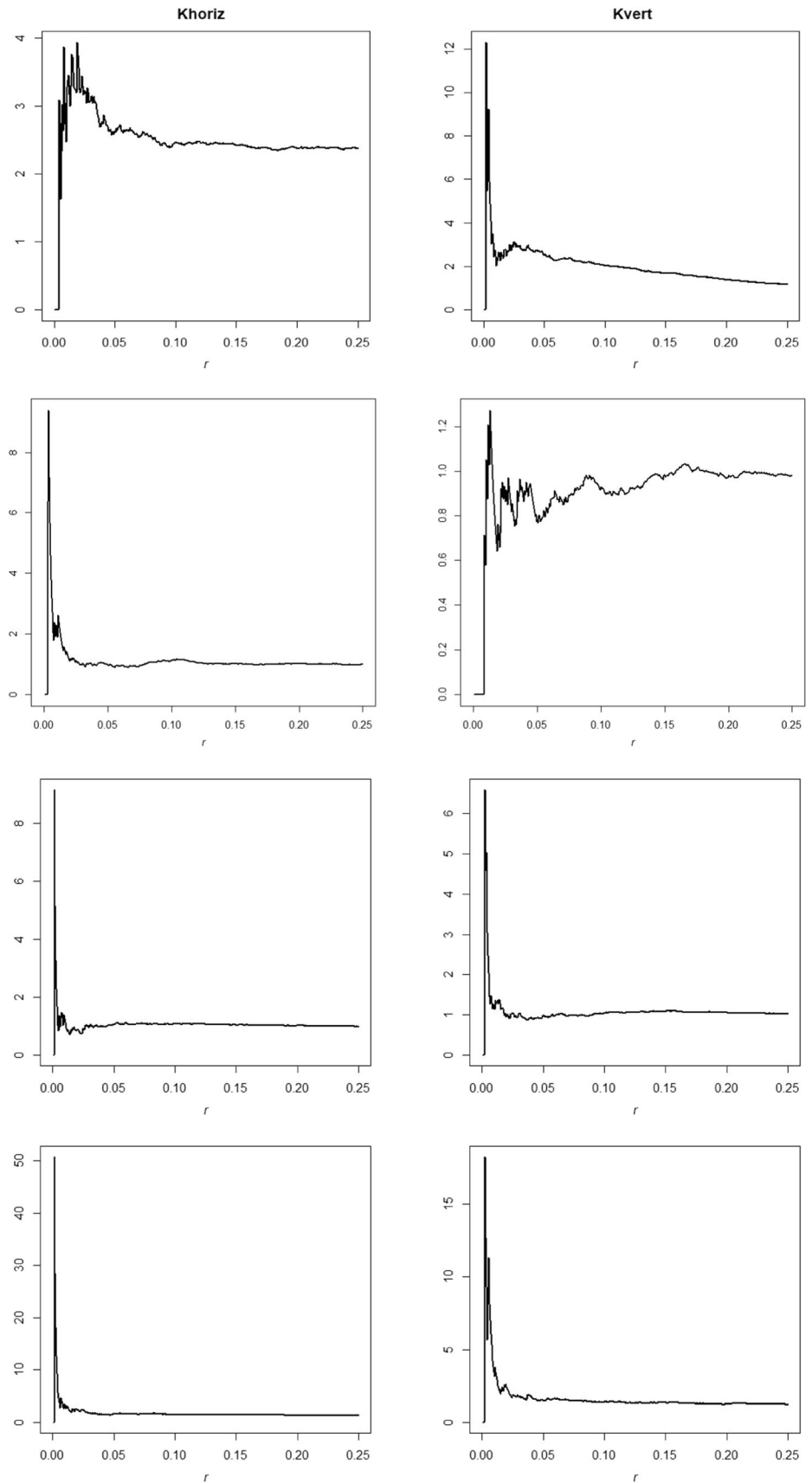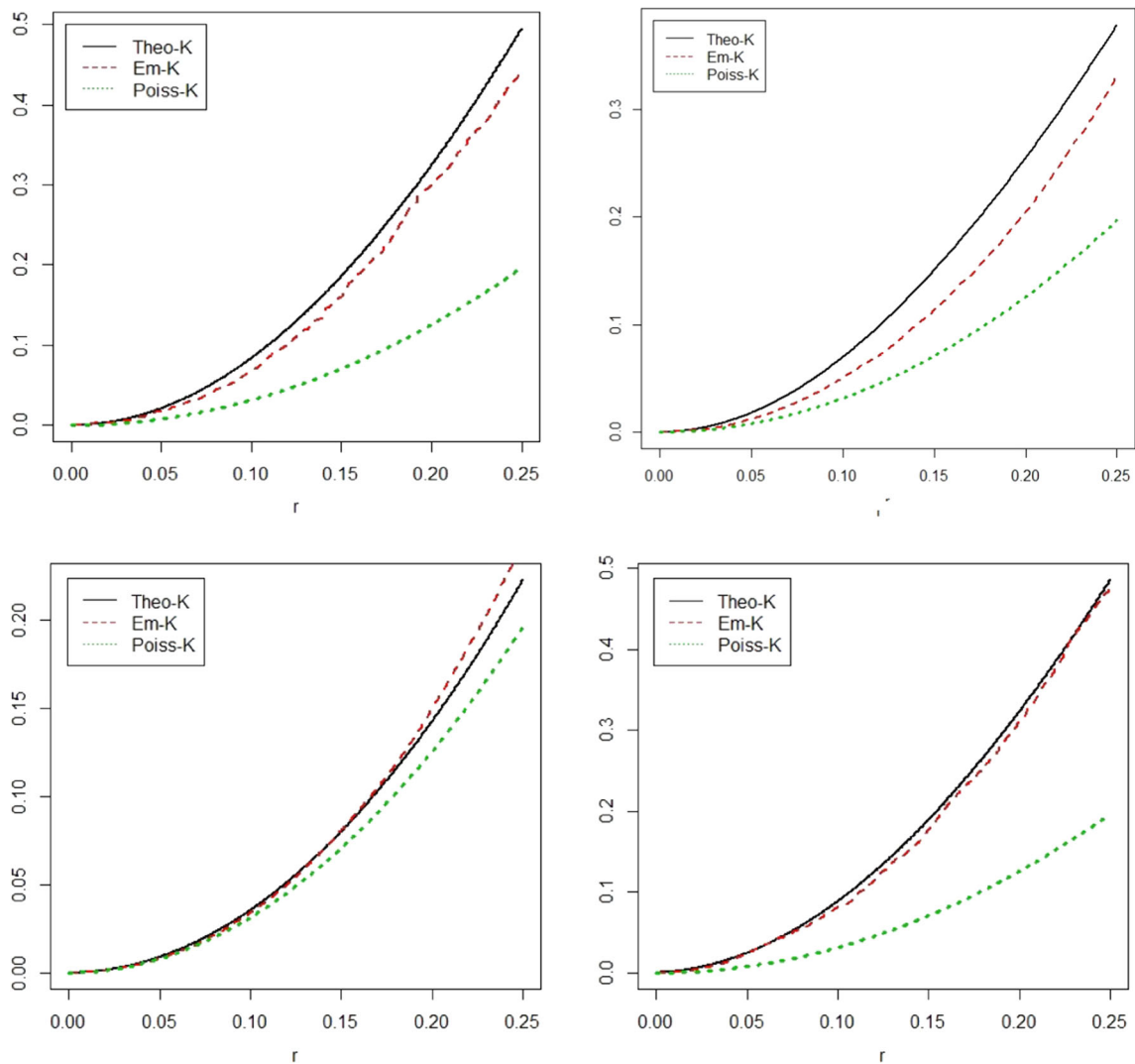
Fig. 7 Comparison of empirical *K*-functions (Em-K) with theoretical ones (Theo-K) over a disc for *Models 1–4,First row*: *Model 1* and *Model 2*, and *Second row*: *Model 3* and *Model 4* (from left to right, respectively), and with the *K*-function under a Poisson point process (Poiss-K)

simulated patterns based on the empirical empty-space *F*-functions providing a 95% confidence interval (Baddeley et al. 2015), and compared them with the empirical *F*-function from the data. We mark two points here. The goodness-of-fit is done through the *F*-functions to avoid using the same *K*-functions in both fitting and assessing goodness-of-fit. Also, we have used 39 simulations following Baddeley *et al.* (2015, page 401) to achieve a %95-confidence interval, using the suggested formula $\frac{2}{m+1}$, where *m* is the number of simulations. However, we have also run model checking under $m = 99$ simulations and the results remain basically unchanged.

As shown in Fig. 15, the empirical *F*-function runs within the envelopes indicating that both models provide a good fit, and thus represent good theoretical models for the earthquake events in South America.

6.2 Analysis of earthquakes in the Mediterranean Europe

The second dataset corresponds to earthquake events in the Mediterranean Europe with magnitude equal or larger than 4 that occurred between January 1950 and June 1998 within a rectangular region of latitude between 30S and 50N, and longitude between $-20W$ and $-42E$, containing 211 earthquakes, as shown in Fig. 16.

We again used sector *K*-functions to assess for possible anisotropic behavior (see Fig. 17). Both sector *K*-functions clearly differ indicating the existence of such anisotropic condition.

We estimated the intensity function using the non-parametric kernel estimator given by (27) together with the *K*-function in (29). Again, after fitting all four models, we only report here those that provided a good fit. We fitted

Table 1 Point estimations, mean absolute percentage error (MAPE), mean squared error (MSE), standard deviations (SD), and confidence intervals (CI) of the estimated parameters for *Models 1–4*

Models	Model 1	Model 2	Model 3	Model 4
Parameters				
α	–	–	2	–
β	–	1	1	–
σ_1	0.05	0.2	3.5	4
σ_2	0.8	0.045	1.7	2
σ^2	–	–	–	1
Point estimations				
$\widehat{\alpha}$	–	–	2.009	–
$\widehat{\sigma}_1$	0.04956	0.19979	3.50115	3.96073
$\widehat{\sigma}_2$	0.79477	0.04485	1.71045	2.00761
$\widehat{\sigma^2}$	–	–	–	1.00073
MAPE				
$\widehat{\alpha}$	–	–	0.0334	–
$\widehat{\sigma}_1$	0.18089	0.01797	0.00985	0.35484
$\widehat{\sigma}_2$	0.06454	0.03456	0.04382	0.15852
$\widehat{\sigma^2}$	–	–	–	0.17878
MSE				
$\widehat{\alpha}$	–	–	0.00663	–
$\widehat{\sigma}_1$	0.00012	0.00003	0.00162	1.462796
$\widehat{\sigma}_2$	0.00407	0.000004	0.00808	0.07489
$\widehat{\sigma^2}$	–	–	–	0.02141
SD				
$\widehat{\alpha}$	–	–	0.08113	–
$\widehat{\sigma}_1$	0.01081	0.0052	0.04035	0.85539
$\widehat{\sigma}_2$	0.06378	0.00187	0.0895	0.1936
$\widehat{\sigma^2}$	–	–	–	0.10359
CI				
$\widehat{\alpha}_1$	–	–	(1.99775, 2.02025)	–
$\widehat{\sigma}_1$	(0.04806, 0.05106)	(0.19906, 0.20051)	(3.49556, 3.50675)	(3.84217, 4.07928)
$\widehat{\sigma}_2$	(0.78593, 0.80361)	(0.04459, 0.04511)	(1.69804, 1.72286)	(1.98077, 2.03444)
$\widehat{\sigma^2}$	–	–	–	(0.98636, 1.01508)

Models 1,4 and used the least square method to estimate the anisotropic parameters. The optimum values were $\hat{\sigma}_1 = 0.028339$ and $\hat{\sigma}_2 = 0.25123$ for *Model 1*, and $\hat{\sigma}_1 = 0.031325$, $\hat{\sigma}_2 = 1.2125454$ and $\sigma^2 = 0.0031565$ for *Model 4*.

Figure 18 depicts the empirical and theoretical *K*-functions together with that under Poissoness. There is an indication of clustering.

We finally proceeded to formally assess the goodness-of-fit of both models, and simulated 39 point patterns with the estimated parameters coming from the fit of *Model 1* and *Model 4* to the events. The envelopes were obtained using *F*-functions as in the previous data analysis. Figure 19 shows that the empirical *F*-function runs within the envelopes indicating that both models provide a good theoretical model for the earthquakes events in the Mediterranean Europe.

Fig. 8 Histograms and boxplots for the estimation of σ_1 (*Top block*) and σ_2 (*Bottom block*) using the minimum contrast method over a disc. *First column*: Model 1 case, *Second column*: Model 2 case
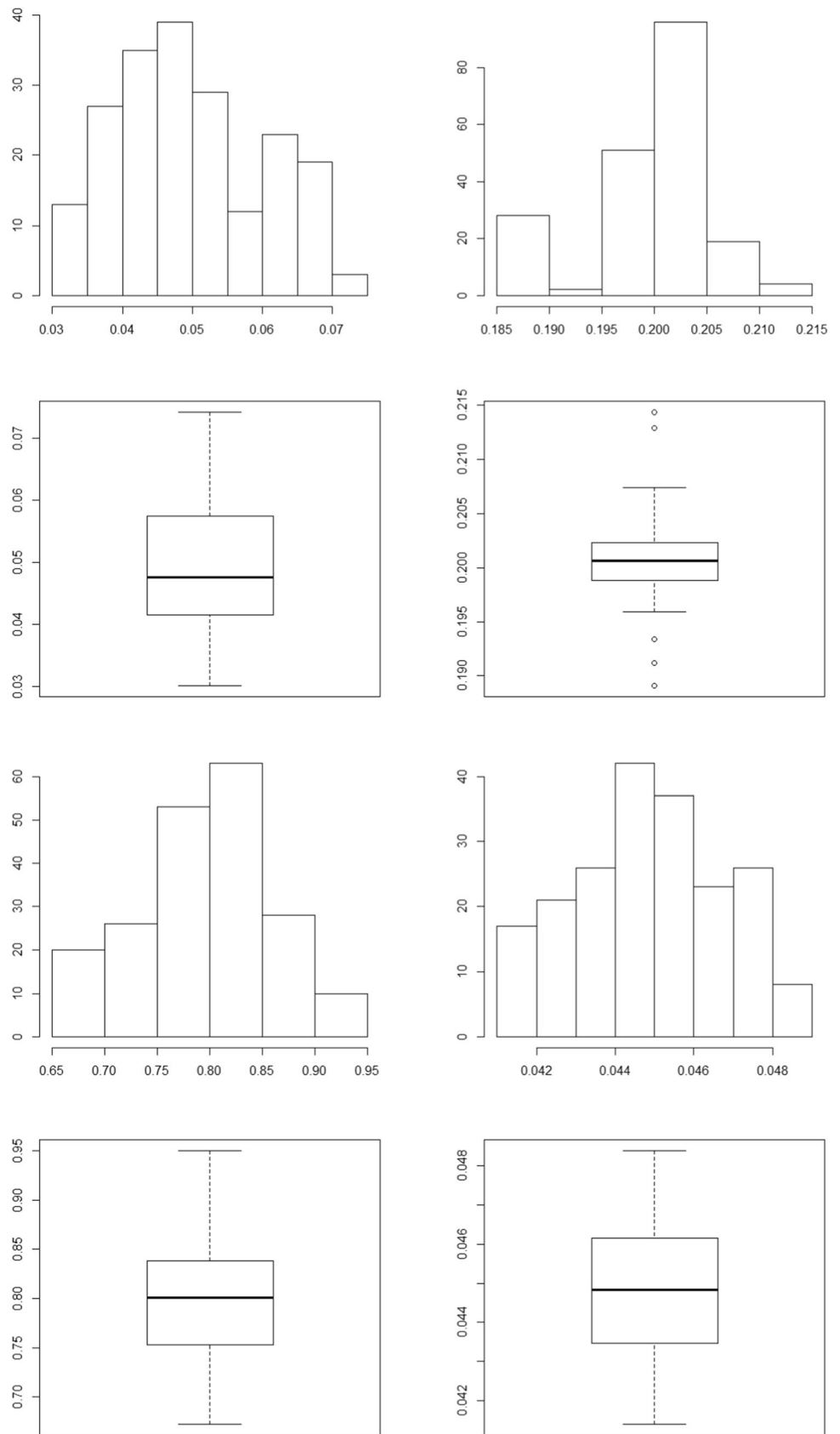
Fig. 9 Histograms and boxplots for the estimation of the parameters using the minimum contrast method over a disc. *First column*: Plots for the estimation of σ_1 (*Top block*), σ_2 (*Center block*), and α (*Bottom block*), for *Model 3*. *Second column*: Plots for the estimation of σ_1 (*Top block*), σ_2 (*Center block*), and σ^2 (*Bottom block*), for *Model 4*
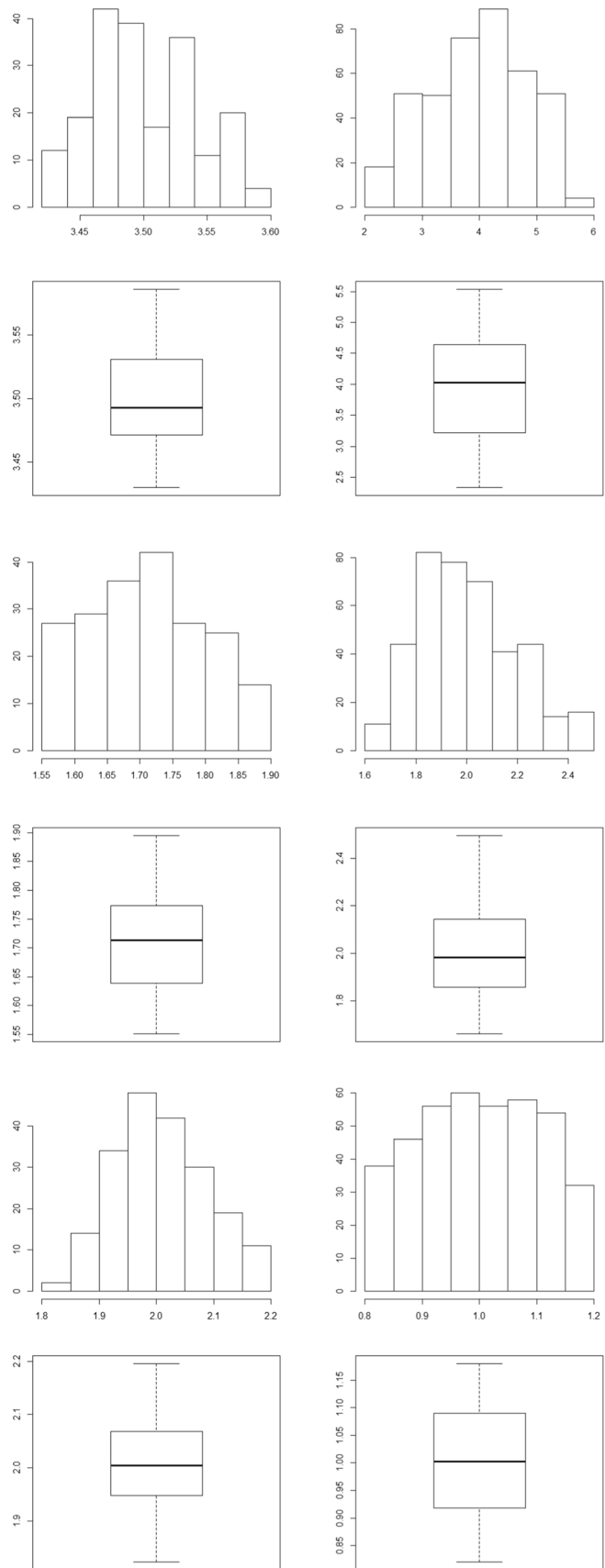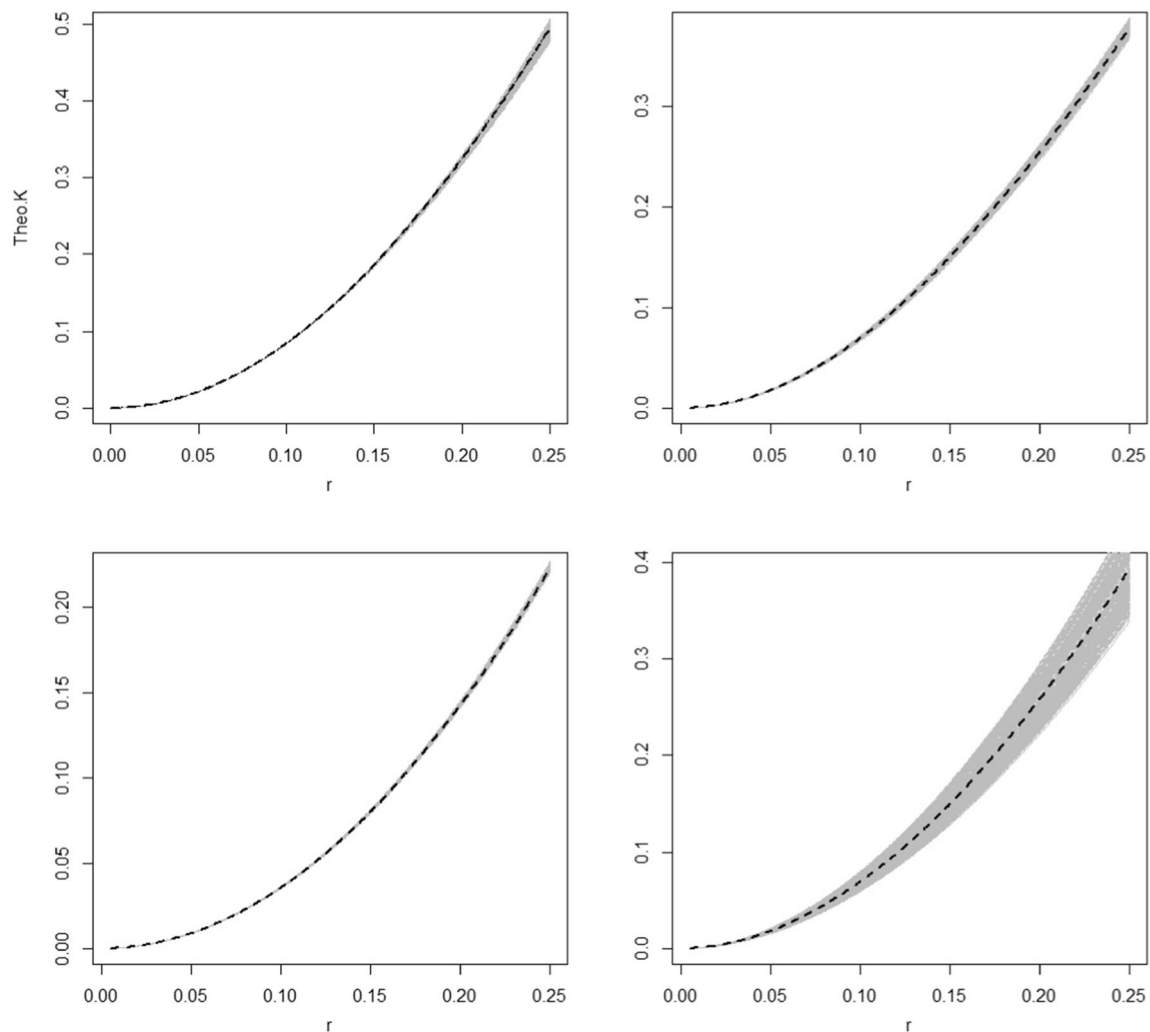
Fig. 10 Theoretical *K*-function based on the true value of parameters (black color) and theoretical *K*-function based on the point estimations (gray color) for each *Model 1–4*, *First row*: *Model 1* and *Model 2*, and *Second row*: *Model 3* and *Model 4*, from left to right, respectively

7 Conclusions and discussion

LGCPs provide a useful class of models, not only for point process data but also for any problem involving the prediction of an incompletely observed spatial (or spatio-temporal) process, irrespective of data format. There are still open developments in statistical computation, parameter estimation, and probabilistic prediction for relatively large data sets, and for particular structural behavior, such as when main directions are present in the point pattern. In particular, areas of current methodological research are the formulation of models and methods for principled statistical analysis that handle anisotropy in a routinely way.

We have introduced some new classes of elliptical and non-elliptical anisotropic LGCP models for modeling anisotropic spatial point patterns that exhibit a certain degree of clustering. The former class of models can be reduced to isotropic forms after some rotations. The latter family is beyond this property and is not reducible to isotropic forms after a rotation. We used two strategies to build these new classes of LGCPs, providing some anisotropic characteristics. The first strategy provides some anisotropic covariance functions and then build the anisotropic LGCP in terms of these covariance functions. This strategy uses two methods. The first method uses the convolution of anisotropic kernel functions, while the second method obtains
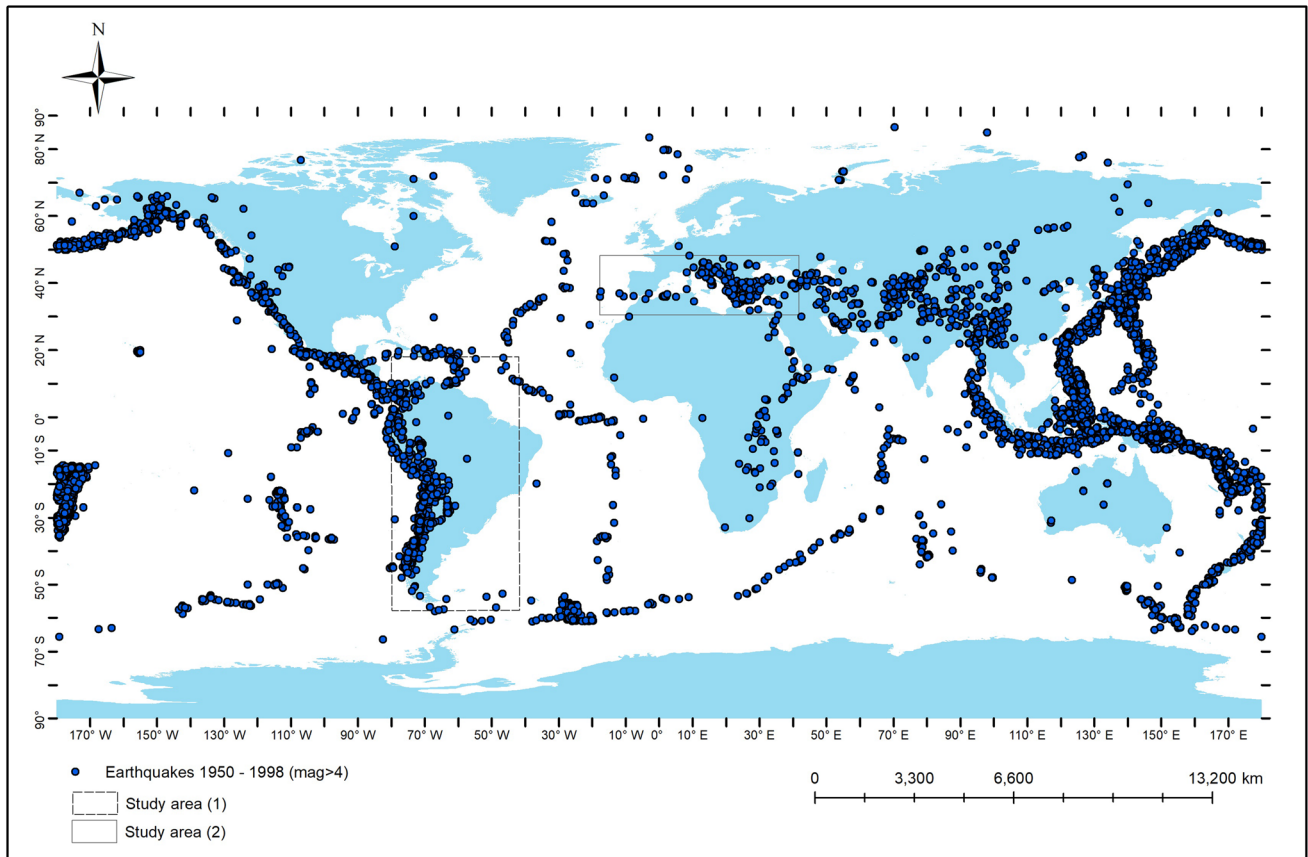
Fig. 11 Locations of earthquakes in the selected regions of South America and the Mediterranean Europe
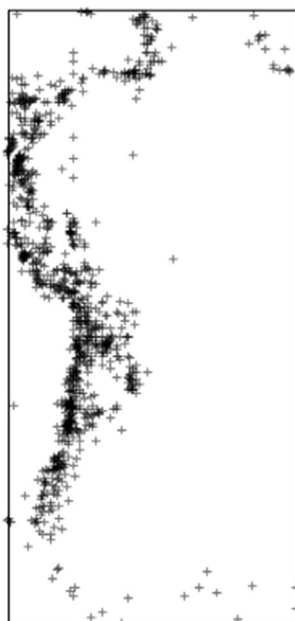

Fig. 12 Locations of earthquakes with magnitude equal or larger than 4 in South America, occurred between January 1950 and June 1998 within a rectangular region of latitude between $-58S$ and $18N$, and longitude between $-80W$ and $-40E$

the anisotropic covariance function through normal variance mixture functions. The second strategy builds the anisotropic LGCP in terms of a non-elliptical anisotropic covariance function. The second-order properties of these models can be studied easily since the pair correlation functions have closed and tractable analytical forms. The new classes are easy to estimate using a method of moments.

This paper contributes to the literature enlarging the family of LGCPs when modeling anisotropic behavior. In a more practical aspect, we found two good models for earthquake events.

We have studied the second-order characteristics of our model over a centred disc with radius ρ, denoted by $A = C(0, \rho)$. However, following Ohser and Stoyan (1981), Illian et al. (2008), and Baddeley et al. (2015), other convenient choices could consider A as a sector of a disc, which is the part of the disc of radius ρ lying between two lines at orientations θ_0 and θ_1, or a sector-ring of a disc, i.e., the sector between two discs, one with radius ρ_1 and the other with radius ρ_2, where $0 \leq \rho_1, \rho_2 < \rho$. The properties of our LGCP models over these bounded sets can be easily obtained with the same calculations. This is a valuable topic of coming research for anisotropic LGCPs.
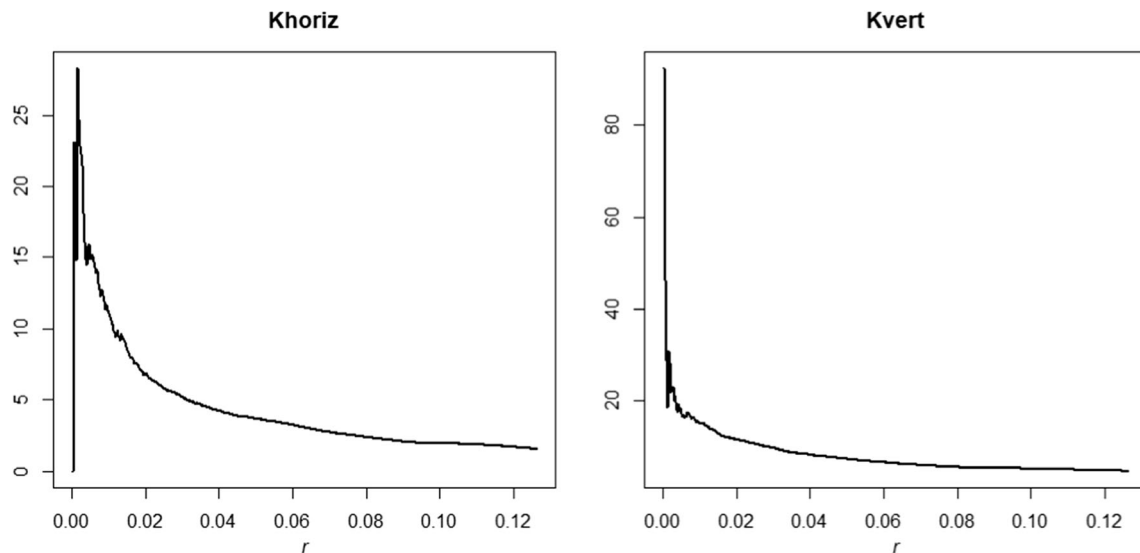
Fig. 13 Anisotropy analysis using sector K-functions for South America earthquake events depicted in Fig. 12. *Left*: Sector K-function for a 30° angle centred on the horizontal axis. *Rigth*: Sector K-function for a 30° angle centred on the vertical axis
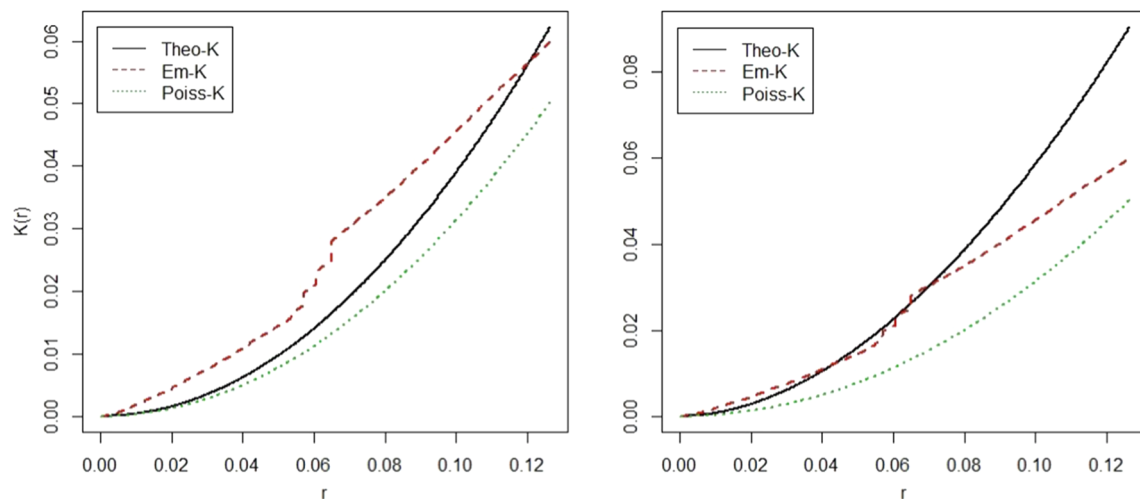
Fig. 14 Empirical K-function for the South America earthquake events (red line), K-function under a Poisson point process (green line), and theoretical K-functions (black) under *Model 1* (*left*), and *Model 4* (*right*)

We have restricted to univariate classes of spatial patterns. However, the extension to the spatio-temporal case and to the multivariate one in the context of anisotropic LGCPs will be a welcome line of research. We note that the log-linear formulation of a LGCP is convenient because of the tractable moment properties of the log-Gaussian distribution. In the extension to spatio-temporal models, we represent the data as the locations, x_i, and the corresponding times, t_i, by $\{(x_i, t_i); \; i = 1, \cdots, n\}$, where each $(x_i, t_i) \in \mathbb{S} \times T$ for some defined spatial region $\mathbb{S}$ and continuous time-interval T. A spatio-temporal anisotropic LGCP is defined as a spatio-temporal Cox process driven by the realization of a random intensity function $\Lambda(x, t) = \exp\{Z(x, t)\}$, where $Z(.)$ is an anisotropic Gaussian process with mean μ, variance σ^2, and covariance function $C(., .)$. The covariance function can be considered
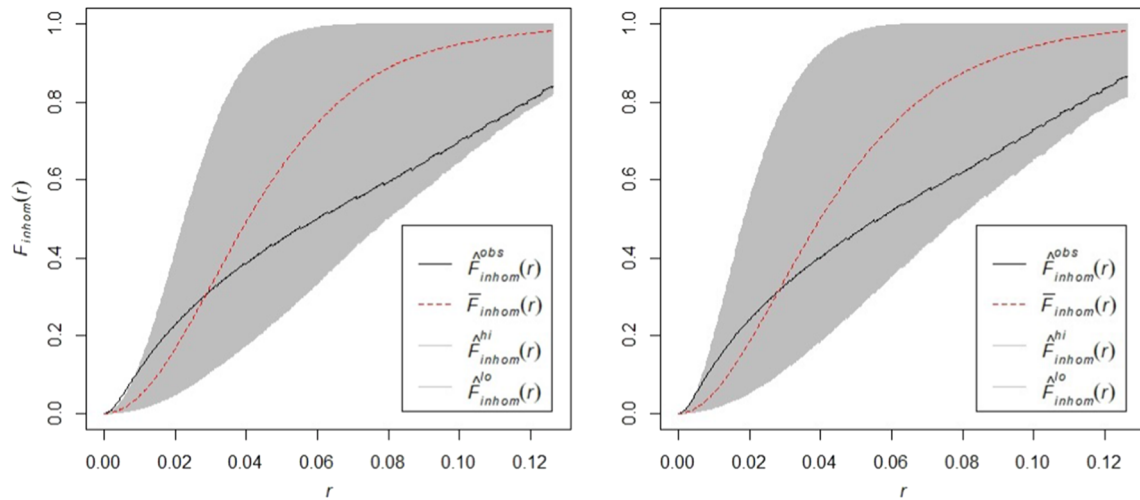
Fig. 15 Envelopes based on the F-function for the earthquake events in South America. Empirical function comes in black, and the pointwise envelopes (shaded region) are obtained from simulations of the LGCP of *Model 1* (*left*), and *Model 4* (*right*). The red line represents a mean *F*-function from the simulations
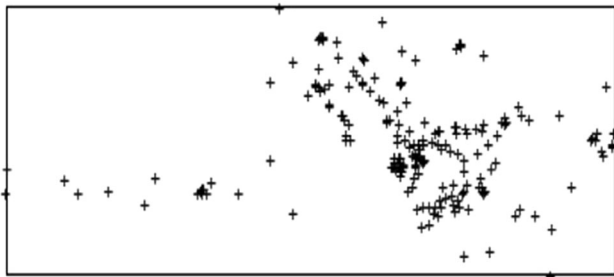

Fig. 16 Locations of earthquake events with magnitude equal or larger than 4 in the Mediterranean Europe, occurred between January 1950 and June 1998 within a rectangular region of latitude between 30S and 50N, and longitude between −20W and −42E

as a separable or non-separable function. Then, we can follow all the steps by changing the spatial points to spatio-temporal ones.

In the spatio-temporal context, it also gives the model a natural interpretation as a multiplicative decomposition of the overall intensity into deterministic and stochastic components. However, it can lead to very highly skewed marginal distributions, with large patches of near-zero intensity interspersed with sharp peaks. This is again a topic that is worth of coming research for spatio-temporal LGCPs exhibiting some kind of anisotropy.
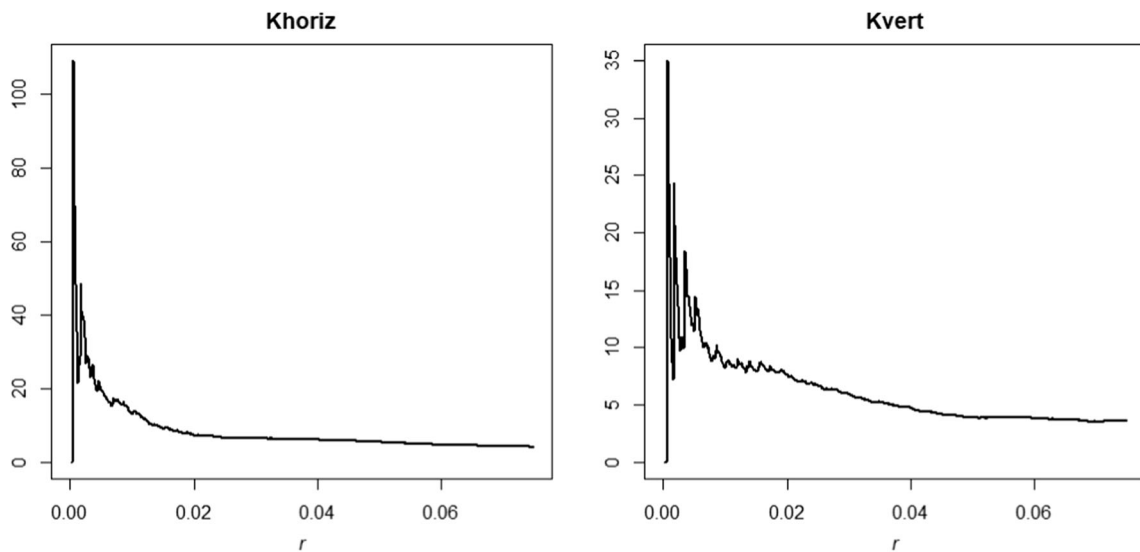
Fig. 17 Anisotropy analysis using sector *K*-functions for the Mediterranean Europe earthquake events depicted in Figure 16. *Left*: Sector *K*-function for a 30° angle centred on the horizontal axis. *Rigth*: Sector *K*-function for a 30° angle centred on the vertical axis
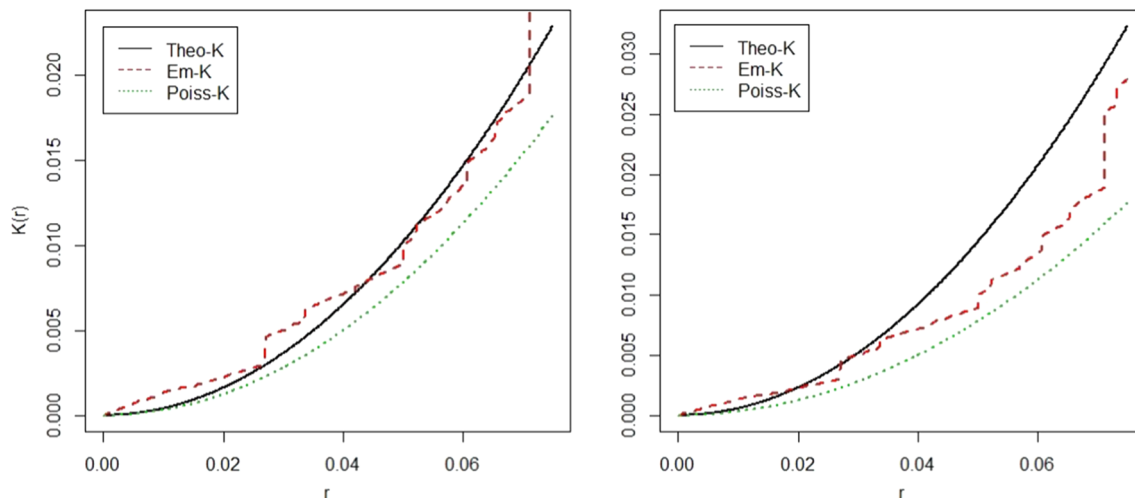
Fig. 18 Empirical K-function for the Mediterranean Europe earthquake events (red line), K-function under a Poisson point process (green line), and theoretical K-functions (black) under *Model 1* (*left*), and *Model 4* (*right*)
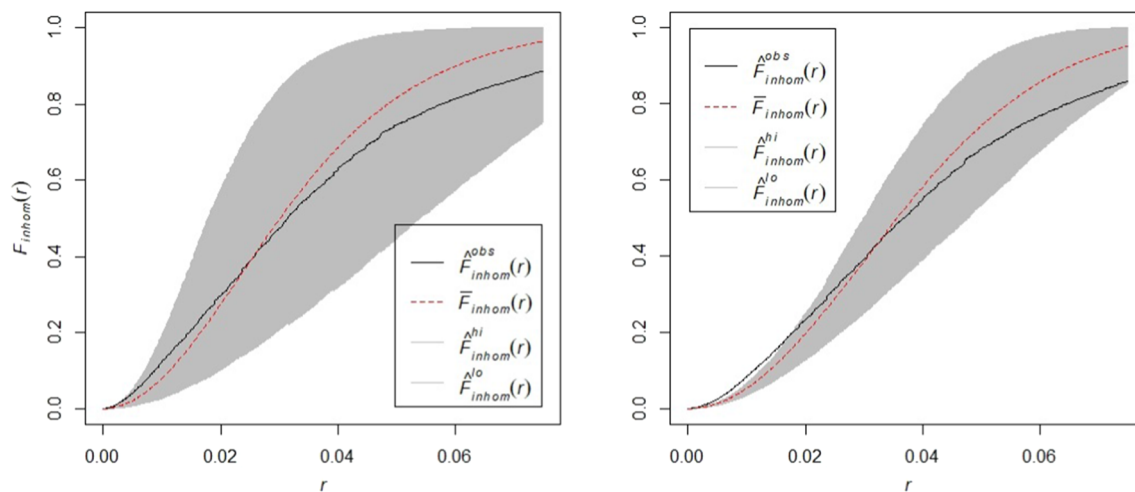
Fig. 19 Envelopes based on the F-function for the earthquake events in the Mediterranean Europe. Empirical function comes in black, and the pointwise envelopes (shaded region) are obtained from simulations of the LGCP of *Model 1* (*left*), and *Model 4* (*right*). The red line represents a mean F-function from the simulations

Appendix

This Appendix considers some calculations for Models 1–4 under the case of A being an ellipse, or a part of an ellipse (for example, a sector-ellipse or a ring of an ellipse).

In obtaining the second-order properties of *Models 1–3*, since the covariance functions have an elliptical form, we here also consider A an ellipse, or a part of an ellipse (a sector-ellipse or a ring of an ellipse). In the elliptical set, as we have the condition $\frac{u_1^2}{a^2} + \frac{u_2^2}{b^2} \leq \rho^2$, we are only successful in obtaining the close form for K-functions when a and b are written in terms of the unknown anisotropic parameters σ_1 and σ_2. Also, the same calculations for Model 4, with an exponential super-ellipse covariance function, were done with considering A as a super-ellipse with the form $|\frac{u_1}{a}|^2 + |\frac{u_2}{b}|^2 \leq \rho^2$, where a and b are equal to the unknown anisotropic parameters σ_1 and σ_2.

Although all calculations coming in the Appendix show close forms for the K-functions, we have preferred shifting them here as the obtained close forms depend on the unknown parameters.

Model 1

K-function over an ellipse.

In (7), we considered A as an ellipse centred at the origin with semi-minor and semi-major axes $a = 2\sqrt{\sigma_1}\rho$ and $b = 2\sqrt{\sigma_2}\rho$, denoted by $A = E(0, a, b)$. The anisotropic K-function over A, denoted here as $K_{aniso}^E(\rho)$, is given by

$$K_{aniso}^E(\rho) = \iint\limits_{\frac{u_1^2}{4\sigma_1} + \frac{u_2^2}{4\sigma_2} \le \rho^2} g(u_1, u_2) du_1 du_2. \tag{30}$$

Substitution of (5) into (30) gives

$$K_{aniso}^E(\rho) = \iint\limits_{\frac{u_1^2}{4\sigma_1} + \frac{u_2^2}{4\sigma_2} \le \rho^2} \exp\left\{\pi\sqrt{\sigma_1\sigma_2}\exp\left\{-\frac{u_1^2}{4\sigma_1} - \frac{u_2^2}{4\sigma_2}\right\}\right\} du_1 du_2.$$

Then, applying a change of variables to the polar coordinate transformation $u_1 = 2\sqrt{\sigma_1}r\cos\theta$ and $u_2 = 2\sqrt{\sigma_2}r\sin\theta$ with $0 \le r \le \rho$ and $0 \le \theta \le 2\pi$. The Jacobean is thus $4r\sqrt{\sigma_1\sigma_2}$. So,

$$K_{aniso}^E(\rho) = \int_0^{2\pi}\int_0^\rho 4\sqrt{\sigma_1\sigma_2} \\ \exp\left\{\pi\sqrt{\sigma_1\sigma_2}\exp\left\{-r^2\right\}\right\} r dr d\theta. \tag{31}$$

Using Maclaurin series, a closed form for the K-function is given by

$$\begin{aligned} K_{aniso}^E(\rho) &= \int_0^{2\pi}\int_0^\rho 4\sqrt{\sigma_1\sigma_2}\sum_{n=0}^\infty \\ &\quad \frac{\left(\pi\sqrt{\sigma_1\sigma_2}\exp\left\{-r^2\right\}\right)^n}{n!} r dr d\theta \\ &= \sum_{n=0}^\infty \frac{4\sqrt{\sigma_1\sigma_2}\left(\pi\sqrt{\sigma_1\sigma_2}\right)^n}{n!} \\ &\quad \int_0^{2\pi}\int_0^\rho \exp\left\{-nr^2\right\} r dr d\theta \\ &= 4\pi\sqrt{\sigma_1\sigma_2}\rho^2 + \sum_{n=1}^\infty \frac{4\left(\pi\sqrt{\sigma_1\sigma_2}\right)^{n+1}}{n.n!} \\ &\quad \left(1 - \exp\left\{-n\rho^2\right\}\right). \end{aligned} \tag{32}$$

By the Ratio Test, it can be proved that the series in (32) converges absolutely, and hence will converge. In a more explicit expression, if we write $a_n = \frac{\left(\pi\sqrt{\sigma_1\sigma_2}\right)^{n+1}}{n.n!}\left(\exp\left\{-n\rho^2\right\} - 1\right)$, then

$$\begin{aligned} \lim_{n\to\infty}\left|\frac{a_{n+1}}{a_n}\right| &= \lim_{n\to\infty}\left|\frac{\frac{\left(\pi\sqrt{\sigma_1\sigma_2}\right)^{n+2}}{(n+1).(n+1)!}\left(\exp\left\{-(n+1)\rho^2\right\} - 1\right)}{\frac{\left(\pi\sqrt{\sigma_1\sigma_2}\right)^{n+1}}{n.n!}\left(\exp\left\{-n\rho^2\right\} - 1\right)}\right| \\ &= \lim_{n\to\infty}\left|\frac{n\pi\sqrt{\sigma_1\sigma_2}\left(\exp\left\{-(n+1)\rho^2\right\} - 1\right)}{(n+1)^2\left(\exp\left\{-n\rho^2\right\} - 1\right)}\right| \\ &= \alpha\pi\lim_{n\to\infty}\left|\frac{n\exp\left\{-(n+1)\rho^2\right\}}{(n+1)^2\left(\exp\left\{-n\rho^2\right\} - 1\right)}\right. \\ &\quad \left. - \frac{n}{(n+1)^2\left(\exp\left\{-n\rho^2\right\} - 1\right)}\right| \\ &\le \pi\sqrt{\sigma_1\sigma_2}\lim_{n\to\infty}\left\{\left|\frac{n\exp\left\{-(n+1)\rho^2\right\}}{(n+1)^2\left(\exp\left\{-n\rho^2\right\} - 1\right)}\right|\right. \\ &\quad \left. + \left|\frac{n}{(n+1)^2\left(\exp\left\{-n\rho^2\right\} - 1\right)}\right|\right\}. \end{aligned}$$

The first part at the right-hand side converges to zero because

$$\begin{aligned} &\lim_{n\to\infty}\left|\frac{n\exp\left\{-(n+1)\rho^2\right\}}{(n+1)^2\left(\exp\left\{-n\rho^2\right\} - 1\right)}\right| \\ &= \lim_{n\to\infty}\frac{n}{(n+1)^2}\cdot\frac{\exp\left\{-(n+1)\rho^2\right\}}{\left(\exp\left\{-n\rho^2\right\} - 1\right)} \\ &= \lim_{n\to\infty}\frac{n}{(n+1)^2} \\ &\quad \times \lim_{n\to\infty}\frac{\exp\left\{n\rho^2\right\}}{\left(\exp\left\{n\rho^2\right\}\exp\left\{\rho^2\right\} - \exp\left\{n\rho^2\right\}\exp\left\{(n+1)\rho^2\right\}\right)} = 0. \end{aligned}$$

The second part again converges to zero using L'Hopital rule,

$$\begin{aligned} &\lim_{n\to\infty}\left|\frac{n}{(n+1)^2\left(\exp\left\{-n\rho^2\right\} - 1\right)}\right| \\ &= \lim_{n\to\infty}\frac{1}{\frac{2(n+1)}{\exp\left\{n\rho^2\right\}} - 2(n+1) - \rho^2\frac{(n+1)^2}{\exp\left\{n\rho^2\right\}}} = 0, \end{aligned}$$

since

$$\lim_{n\to\infty}\frac{2(n+1)}{\exp\left\{n\rho^2\right\}} = 0, \quad \lim_{n\to\infty}2(n+1) = \infty,$$

$$\lim_{n\to\infty}\rho^2\frac{(n+1)^2}{\exp\left\{n\rho^2\right\}} = 0.$$

Thus $\lim_{n\to\infty}\left|\frac{a_{n+1}}{a_n}\right|$ is less than 1, and the series defined in (32) for $K_{aniso}^E(\rho)$ converges.

K-function over a sector-ellipse.

As a second case, we consider A a sector of an ellipse, i.e., the part of an ellipse lying between two lines at orientations θ_0 and θ_1. For the sector-ellipse K-function, denoted as

$K_{aniso}^{SE}(\cdot)$, since the upper bound of the inner polar integral in (31) does not depend on the angles, we only used the angles $\theta_0 \le \theta \le \theta_1$ instead of $0 \le \theta \le 2\pi$, and obtained

$$
\begin{aligned}
K_{aniso}^{SE}(\rho) &= \int_{\theta_0}^{\theta_1} \int_0^{\rho} 4\sqrt{\sigma_1 \sigma_2} \\
&\quad \exp\left\{\pi\sqrt{\sigma_1 \sigma_2}\exp\left\{-r^2\right\}\right\} r\,dr\,d\theta \\
&= 2(\theta_1 - \theta_0)\sqrt{\sigma_1 \sigma_2}\rho^2 \\
&\quad + \sum_{n=1}^{\infty} \frac{(\theta_1 - \theta_0)\left(\pi\sqrt{\sigma_1\sigma_2}\right)^n \sqrt{\sigma_1\sigma_2}^n}{n.n!} \\
&\quad \times \left(1 - \exp\left\{-n\rho^2\right\}\right).
\end{aligned}
\tag{33}
$$

The K-function over a sector-ring of an ellipse

As a final case, we considered A a sector-ring of an ellipse. We assumed A_1 is a sector-ellipse centred at the origin with semi-minor and semi-major axes $a_1 = 2\sqrt{\sigma_1}\rho_1$ and $b_1 = 2\sqrt{\sigma_2}\rho_1$, and A_2 a sector-ellipse centred at the origin with semi-minor and semi-major axes $a_2 = 2\sqrt{\sigma_1}\rho_2$ and $b_2 = 2\sqrt{\sigma_2}\rho_2$, both lying between two lines at constant orientations θ_0 and θ_1 and $\rho_1 < \rho_2$. With considering A a sector-ring lying between the sector-ellipse of A_1 and the sector-ellipse of A_2, the anisotropic K-function over A, denoted by $K_{aniso}^{SRE}(\rho_1, \rho_2)$ is obtained as

$$
\begin{aligned}
&K_{aniso}^{SRE}(\rho_1, \rho_2) \\
&= K_{aniso}^{SE}(\rho_2) \setminus K_{aniso}^{SE}(\rho_1) \\
&= \int_{\theta_0}^{\theta_1} \int_0^{\rho_2} 4\sqrt{\sigma_1\sigma_2}\exp\left\{\pi\sqrt{\sigma_1\sigma_2}\exp\left\{-r^2\right\}\right\}r\,dr\,d\theta \\
&\quad - \int_{\theta_0}^{\theta_1} \int_0^{\rho_1} 4\sqrt{\sigma_1\sigma_2}\exp\left\{\pi\sqrt{\sigma_1\sigma_2}\exp\left\{-r^2\right\}\right\}r\,dr\,d\theta \\
&= 2(\theta_1 - \theta_0)\sqrt{\sigma_1\sigma_2}\rho_2^2 \\
&\quad + \sum_{n=1}^{\infty}\frac{(\theta_1-\theta_0)\left(\pi\sqrt{\sigma_1\sigma_2}\right)^n\sqrt{\sigma_1\sigma_2}^n}{n.n!}\left(1-\exp\left\{-n\rho_2^2\right\}\right) \\
&\quad - 2(\theta_1 - \theta_0)\sqrt{\sigma_1\sigma_2}\rho_1^2 \\
&\quad - \sum_{n=1}^{\infty}\frac{(\theta_1-\theta_0)\left(\pi\sqrt{\sigma_1\sigma_2}\right)^n\sqrt{\sigma_1\sigma_2}^n}{n.n!}\left(1-\exp\left\{-n\rho_1^2\right\}\right) \\
&= 2(\theta_1 - \theta_0)\sqrt{\sigma_1\sigma_2}(\rho_2^2 - \rho_1^2) \\
&\quad + \sum_{n=1}^{\infty}\frac{(\theta_1-\theta_0)\left(\pi\sqrt{\sigma_1\sigma_2}\right)^n\sqrt{\sigma_1\sigma_2}^n}{n.n!} \\
&\quad \times \left(\exp\left\{-n\rho_1^2\right\} - \exp\left\{-n\rho_2^2\right\}\right).
\end{aligned}
$$

Model 2

The K-function over an ellipse

In Model 2, the anisotropic K-function over the centred ellipse $A = E(0, a, b)$ with semi-minor and semi-major axes $a = 2\sqrt{\sigma_1\beta}\rho$ and $b = 2\sqrt{\sigma_2\beta}\rho$, denoted by $K_{aniso}^{E}(.)$, is obtained by combination of Eqs. (7) and (21), as follows

$$
\begin{aligned}
K_{aniso}^{E}(\rho) &= \iint_{\frac{u_1^2}{2\sigma_1\beta}+\frac{u_2^2}{2\sigma_2\beta}\le\rho^2} \exp\left\{\frac{1}{4\pi\beta\sqrt{\sigma_1\sigma_2}}\right. \\
&\quad \left. \left[1 + \frac{u_1^2}{2\sigma_1\beta} + \frac{u_2^2}{2\sigma_2\beta}\right]^{-\frac{3}{2}}\right\}du_1 du_2.
\end{aligned}
$$

Using polar coordinates and the Taylor expansion, the closed form of the K-function is given by

$$
\begin{aligned}
&K_{aniso}^{E}(\rho) \\
&= 2\beta\sqrt{\sigma_1\sigma_2}\int_0^{2\pi}\int_0^{\rho}\exp\left\{\frac{1}{4\pi\beta\sqrt{\sigma_1\sigma_2}}[1+r^2]^{-\frac{3}{2}}\right\}r\,dr\,d\theta \\
&= 4\pi\beta\sqrt{\sigma_1\sigma_2}\int_0^{\rho}\sum_{n=0}^{\infty}\frac{\left\{\frac{1}{4\pi\beta\sqrt{\sigma_1\sigma_2}}[1+r^2]^{-\frac{3}{2}}\right\}^n}{n!}r\,dr \\
&= 4\pi\beta\sqrt{\sigma_1\sigma_2}\sum_{n=0}^{\infty}\frac{\left[4\pi\beta\sqrt{\sigma_1\sigma_2}\right]^{-n}}{(2-3n)n!}\left[(1+\rho^2)^{\frac{2-3n}{2}}-1\right] \\
&= \sum_{n=0}^{\infty}\frac{\left[4\pi\beta\sqrt{\sigma_1\sigma_2}\right]^{1-n}}{(2-3n)n!}\left[(1+\rho^2)^{\frac{2-3n}{2}}-1\right].
\end{aligned}
\tag{34}
$$

Using the Ratio Test, it is easy to show that this series converges. Assume that $a_n = \frac{\left[4\pi\beta\sqrt{\sigma_1\sigma_2}\right]^{1-n}}{\frac{2-3n}{2}n!}\left[(1+\rho^2)^{2-3n}-1\right]$, then

$$
\begin{aligned}
\lim_{n\to\infty}\frac{a_{n+1}}{a_n} &= \lim_{n\to\infty}\frac{\frac{\left[4\pi\beta\sqrt{\sigma_1\sigma_2}\right]^{1-(n+1)}}{(2-3(n+1))(n+1)!}\left[(1+\rho^2)^{\frac{2-3(n+1)}{2}}-1\right]}{\frac{\left[4\pi\beta\sqrt{\sigma_1\sigma_2}\right]^{1-n}}{(2-3n)n!}\left[(1+\rho^2)^{\frac{2-3n}{2}}-1\right]} \\
&= \lim_{n\to\infty}\frac{1}{n+1}\cdot\frac{2-3n}{-1-3n}\cdot\left[4\pi\beta\sqrt{\sigma_1\sigma_2}\right]^{-1} \\
&\quad \left[\frac{(1+\rho^2)^{\frac{2-3(n+1)}{2}}-1}{(1+\rho^2)^{\frac{2-3n}{2}}-1}\right] \\
&= 0.
\end{aligned}
$$

The K-function over a sector-ellipse.

We also obtain the sector-ellipse K-function for an angle $\theta_0 \le \theta \le \theta_1$, with semi-minor and semi-major axes $a = 2\sqrt{\sigma_1\beta}\rho$ and $b = 2\sqrt{\sigma_2\beta}\rho$. In particular, K_{aniso}^{SE} is obtained as the form

$$K_{aniso}^{SE}(\rho) = (\theta_1 - \theta_0)(2\beta\sqrt{\sigma_1\sigma_2})^\infty$$
$$\sum_{n=0} \frac{[4\pi\beta\sqrt{\sigma_1\sigma_2}]^{-n}}{(2-3n)n!}[(1+\rho^2)^{\frac{2-3n}{2}} - 1]. \quad (35)$$

Using the same procedure as in (34), this series can be shown to converge.

The *K*-function over a sector-ring of an ellipse

Finally, the anisotropic *K*-function over the sector-ring of an ellipse *A* with $a_1 = 2\sqrt{\sigma_1}\beta\rho_1$, $b_1 = 2\sqrt{\sigma_2}\beta\rho_1$, $a = 2\sqrt{\sigma_1}\beta\rho_2$ and $b = 2\sqrt{\sigma_2}\beta\rho_2$, is given by

$$K_{aniso}^{SRE}(\rho_1, \rho_2) = K_{aniso}^{SE}(\rho_2) \setminus K_{aniso}^{SE}(\rho_1)$$
$$= \int_{\theta_0}^{\theta_1} \int_0^{\rho_2} \exp\left\{\frac{1}{4\pi\beta\sqrt{\sigma_1\sigma_2}}[1+r^2]^{-\frac{3}{2}}\right\} r dr d\theta$$
$$- \int_{\theta_0}^{\theta_1} \int_0^{\rho_1} \exp\left\{\frac{1}{4\pi\beta\sqrt{\sigma_1\sigma_2}}[1+r^2]^{-\frac{3}{2}}\right\} r dr d\theta$$
$$= (\theta_1 - \theta_0)(2\beta\sqrt{\sigma_1\sigma_2}) \sum_{n=0}^\infty \frac{[4\pi\beta\sqrt{\sigma_1\sigma_2}]^{-n}}{(2-3n)n!}[(1+\rho_2^2)^{\frac{2-3n}{2}} - 1]$$
$$- (\theta_1 - \theta_0)(2\beta\sqrt{\sigma_1\sigma_2}) \sum_{n=0}^\infty \frac{[4\pi\beta\sqrt{\sigma_1\sigma_2}]^{-n}}{(2-3n)n!}[(1+\rho_1^2)^{\frac{2-3n}{2}} - 1]$$
$$= (\theta_1 - \theta_0)(2\beta\sqrt{\sigma_1\sigma_2}) \sum_{n=0}^\infty \frac{[4\pi\beta\sqrt{\sigma_1\sigma_2}]^{-n}}{(2-3n)n!}$$
$$\times [(1+\rho_2^2)^{\frac{2-3n}{2}} - (1+\rho_1^2)^{\frac{2-3n}{2}}].$$

providing a convergent series.

Model 3

The *K*-function over an ellipse

Similarly to the previous model, by combining Eqs. (7) and (24), and using polar coordinates and the Taylor expansion, the *K*-function over the ellipse $A = E(0, a, b)$ with semi-minor and semi-major axes $a = 2\sqrt{\sigma_1}\beta\rho$ and $b = 2\sqrt{\sigma_2}\beta\rho$, is obtained as

$$K_{aniso}^E(\rho) = \int_{\|u\| \le \rho} \frac{\alpha}{2\pi\beta\sqrt{\sigma_1\sigma_2}}[1 + \frac{u_1^2}{2\sigma_1\beta} + \frac{u_2^2}{2\sigma_2\beta}]^{-(\alpha+1)} du$$
$$= 2\beta\sqrt{\sigma_1\sigma_2} \int_0^{2\pi} \int_0^\rho \exp\left\{\frac{\alpha}{2\pi\beta\sqrt{\sigma_1\sigma_2}}[1+r^2]^{-(\alpha+1)}\right\} r dr d\theta$$
$$= \sum_{n=0}^\infty \frac{2\alpha^n[2\pi\beta\sqrt{\sigma_1\sigma_2}]^{1-n}}{n!} \int_0^\rho [1+r^2]^{-n(\alpha+1)} r dr$$
$$= \sum_{n=0}^\infty \frac{\alpha^n[2\pi\beta\sqrt{\sigma_1\sigma_2}]^{1-n}}{n!(1-n(\alpha+1))}[(1+\rho^2)^{1-n(\alpha+1)} - 1].$$
$$(36)$$

We can show that this series converges using the Ratio Test, as follows. Let $a_n = \frac{2\beta}{n!}\left[2\pi\sqrt{\sigma_1\sigma_2}\right]^{1-n} \frac{\alpha^n}{2-2n\alpha}[(1+\rho^2)^{1-n\alpha} - 1]$, then

$$\lim_{n\to\infty} \frac{a_{n+1}}{a_n} = \lim_{n\to\infty} \frac{\frac{\alpha^{n+1}}{(n+1)!(1-(n+1)(\alpha+1))}\left[2\pi\beta\sqrt{\sigma_1\sigma_2}\right]^{1-(n+1)}[(1+\rho^2)^{1-(n+1)(\alpha+1)} - 1]}{\frac{\alpha^n}{n!(1-n(\alpha+1))}\left[2\pi\beta\sqrt{\sigma_1\sigma_2}\right]^{1-n}[(1+\rho^2)^{1-n(\alpha+1)} - 1]}$$
$$= \lim_{n\to\infty} \frac{\alpha}{n+1} \cdot \frac{1-n(\alpha+1)}{1-(n+1)(\alpha+1)} \cdot [2\pi\beta\sqrt{\sigma_1\sigma_2}]^{-1}$$
$$\times \left[\frac{(1+\rho^2)^{1-(n+1)(\alpha+1)}}{(1+\rho^2)^{1-n(\alpha+1)} - 1} - \frac{1}{(1+\rho^2)^{1-n(\alpha+1)} - 1}\right]$$
$$= \lim_{n\to\infty} \frac{\alpha}{n+1} \cdot \frac{1-n(\alpha+1)}{1-(n+1)(\alpha+1)} \cdot [2\pi\beta\sqrt{\sigma_1\sigma_2}]^{-1}$$
$$\times \left[\frac{(1+\rho^2)^{1-(\alpha+1)} - (1+\rho^2)^{n(\alpha+1)}}{(1+\rho^2) - (1+\rho^2)^{n(\alpha+1)}}\right]$$
$$= 0.$$

The *K*-function over a sector-ellipse

Here, we now consider *A* as a centred sector-ellipse with semi-minor and semi-major axes $a = 2\sqrt{\sigma_1}\beta\rho$ and $b = 2\sqrt{\sigma_2}\beta\rho$. So, the anisotropic sector-ellipse *K*-function over *A* is given by the convergent series

$$K_{aniso}^{SE}(\rho) = [(\theta_1 - \theta_0)\beta\sqrt{\sigma_1\sigma_2}] \sum_{n=0}^\infty \frac{\alpha^n[2\pi\beta\sqrt{\sigma_1\sigma_2}]^{-n}}{n!(1-n(\alpha+1))}$$
$$\times [(1+\rho^2)^{1-n(\alpha+1)} - 1].$$
$$(37)$$

The *K*-function over a sector-ring of an ellipse

We finally obtain the anisotropic *K*-function over the centred sector-ring of an ellipse with $a_1 = 2\sqrt{\sigma_1}\beta\rho_1$, $b_1 = 2\sqrt{\sigma_2}\beta\rho_1$, $a = 2\sqrt{\sigma_1}\beta\rho_2$ and $b = 2\sqrt{\sigma_2}\beta\rho_2$. The anisotropic sector-ring *K*-function over *A* is given by

$$K_{aniso}^{SRE}(\rho_1, \rho_2) = K_{aniso}^{SE}(\rho_2) \setminus K_{aniso}^{SE}(\rho_1)$$
$$= [(\theta_1 - \theta_0)\beta\sqrt{\sigma_1\sigma_2}] \sum_{n=0}^\infty \frac{\alpha^n[2\pi\beta\sqrt{\sigma_1\sigma_2}]^{-n}}{n!(1-n(\alpha+1))}[(1+\rho_2^2)^{1-n(\alpha+1)} - 1]$$
$$- [(\theta_1 - \theta_0)\beta\sqrt{\sigma_1\sigma_2}] \sum_{n=0}^\infty \frac{\alpha^n[2\pi\beta\sqrt{\sigma_1\sigma_2}]^{-n}}{n!(1-n(\alpha+1))}[(1+\rho_1^2)^{1-n(\alpha+1)} - 1]$$
$$= [(\theta_1 - \theta_0)\beta\sqrt{\sigma_1\sigma_2}]$$
$$\times \sum_{n=0}^\infty \frac{\alpha^n[2\pi\beta\sqrt{\sigma_1\sigma_2}]^{-n}}{n!(1-n(\alpha+1))}[(1+\rho_2^2)^{1-n(\alpha+1)} - (1+\rho_1^2)^{1-n(\alpha+1)}],$$

which, using similar arguments as before, is easy to show that this series converges.

Model 4

The K-function of LGCP over a super-ellipse

Here, we assume that a bounded set A is an area of a superellipse centred at the origin with semi-minor and semi-major axes $a = \sigma_1\rho$ and $b = \sigma_2\rho$, denoted here as $A = SuE(0, a, b)$, with the form

$$\left|\frac{u_1}{a}\right|^{\frac{2}{n}} + \left|\frac{u_2}{b}\right|^{\frac{2}{n}} \leq 1. \tag{38}$$

Substituting (25) into (7) we obtain the K-function of our new model, denoted by $K^{ESE}(.)$, as

$$K^{ESE}(\rho) = \int\int_{\left|\frac{u_1}{\sigma_1}\right|^{\frac{2}{n}} + \left|\frac{u_2}{\sigma_2}\right|^{\frac{2}{n}} \leq \rho^{\frac{2}{n}}} g(u)du_1du_2$$

$$= n\sigma_1\sigma_2\rho^2\frac{\Gamma^2\left(\frac{n}{2}\right)}{\Gamma(n)} + n^2\sigma_1\sigma_2\frac{\Gamma^2\left(\frac{n}{2}\right)}{\Gamma(n)} \tag{39}$$

$$\sum_{k=1}^{\infty}\frac{\sigma^{2k}}{k!k^n}\left(\Gamma(n) - \Gamma\left(n, k\rho^2\right)\right).$$

By the Ratio Test, it can be proved that the series in (39) converge absolutely and hence converge.

Proof The close form of the K-function in (39) and its convergence

First step To reduce the complexity of this proof, we first calculate the four following terms.

The first term

We know that

$$Beta(m + 1, n + 1) = \frac{m!n!}{(m + n + 1)!}.$$

On the other hand, we have

$$m!n! = \int_0^{\infty} e^{-u}u^m du \int_0^{\infty} e^{-v}v^n dv$$

$$= 4\int_0^{\infty} e^{-x^2}x^{2m+1}dx \int_0^{\infty} e^{-y^2}y^{2n+1}dy$$

$$= \int_{-\infty}^{\infty}\int_{-\infty}^{\infty} e^{-x^2+y^2}|x|^{2m+1}|y|^{2n+1}dxdy$$

$$= \int_0^{2\pi}\int_0^{\infty} e^{-r^2}|r\cos(\theta)|^{2m+1}|r\sin(\theta)|^{2n+1}rdrd\theta$$

$$= 4\int_0^{\infty} e^{-r^2}r^{2m+2n+3}dr \int_0^{\frac{\pi}{2}} \cos^{2m+1}(\theta)\sin^{2n+1}(\theta)d\theta$$

$$= 2\int_0^{\infty} e^{-t}t^{m+n+1}dr \int_0^{\frac{\pi}{2}} \cos^{2m+1}(\theta)\sin^{2n+1}(\theta)d\theta$$

$$= 2(m + n + 1)!\int_0^{\frac{\pi}{2}} \cos^{2m+1}(\theta)\sin^{2n+1}(\theta)d\theta.$$

Therefore,

$$\int_0^{\frac{\pi}{2}} \cos^{2m+1}(\theta)\sin^{2n+1}(\theta)d\theta = \frac{m!n!}{2(m + n + 1)!}$$

$$= \frac{Beta(n + 1, m + 1)}{2}.$$

The second term

To obtain the close form for the integral

$$\int_0^{\rho} re^{-kr^{\frac{2}{n}}}dr,$$

we use the changing of variable $kr^{\frac{2}{n}} = t$ and the definition of the Gamma function. So,

$$\int_0^{\rho} re^{-kr^{\frac{2}{n}}}dr = \int_0^{k\rho^{\frac{2}{n}}} \frac{ne^{-t}t^{n-1}}{2k^n}dt$$

$$= \int_0^{\infty} \frac{ne^{-t}t^{n-1}}{2k^n}dt$$

$$- \int_{k\rho^{\frac{2}{n}}}^{\infty} \frac{ne^{-t}t^{n-1}}{2k^n}$$

$$= \frac{n}{2k^n}\left[\Gamma(n) - \Gamma\left(n, k\rho^{\frac{2}{n}}\right)\right].$$

The third term

Here, to obtain the integral

$$\int\int_{\left|\frac{u_1}{\sigma_1}\right|^{\frac{2}{n}} + \left|\frac{u_2}{\sigma_2}\right|^{\frac{2}{n}} \leq \rho^{\frac{2}{n}}} du_1du_2,$$

we use the change of variables $\frac{u_1}{\sigma_1} = t_1$ and $\frac{u_2}{\sigma_2} = t_2$. So

$$\iint\limits_{|t_1|^{\frac{2}{n}}+|t_2|^{\frac{2}{n}} \le \rho^{\frac{2}{n}}} \sigma_1\sigma_2 dt_1 dt_2.$$

The defined super-ellipsoidal shapes are symmetric about the origin of the coordinates, and we substitute the integral with 4 times the integral on the first quadrant of the coordinates. Then, we apply the change of variables formula to the polar coordinate transformation $t_1 = n\cos^n\theta$ and $t_2 = r\sin^n\theta$ with $0 < r < \rho$ and $0 < \theta < 2\pi$. The Jacobean is thus

$$J = \begin{bmatrix} \dfrac{dt1}{dr} & \dfrac{dt1}{d\theta} \\ \dfrac{dt2}{dr} & \dfrac{dt2}{d\theta} \end{bmatrix}$$
$$= \begin{bmatrix} \cos^n\theta & -nr\sin\theta\cos^{n-1}\theta \\ \sin^n\theta & nr\cos\theta\sin^{n-1}\theta \end{bmatrix}$$
$$= nr\cos^{n-1}\theta\sin^{n-1}\theta,$$

Consequently,

$$\iint\limits_{\left|\frac{u_1}{\sigma_1}\right|^{\frac{2}{n}}+\left|\frac{u_2}{\sigma_2}\right|^{\frac{2}{n}} \le \rho^{\frac{2}{n}}} du_1 du_2$$
$$= 4\sigma_1\sigma_2 \iint\limits_{t_1^{\frac{2}{n}}+t_2^{\frac{2}{n}} \le \rho^{\frac{2}{n}};t_1,t_2 \ge 0} dt_1 dt_2$$
$$= 4n\sigma_1\sigma_2 \int_0^{\frac{\pi}{2}}\int_0^{\rho} r\sin^{n-1}(\theta)\cos^{n-1}(\theta)drd\theta$$
$$= 4n\sigma_1\sigma_2 \int_0^{\frac{\pi}{2}} \sin^{n-1}(\theta)\cos^{n-1}(\theta)d\theta \int_0^{\rho} rdr$$
$$= n\sigma_1\sigma_2\rho^2 \frac{\Gamma^2\left(\frac{n}{2}\right)}{\Gamma(n)},$$

The fourth term

Here, we obtain the integral

$$\iint\limits_{\left|\frac{u_1}{\sigma_1}\right|^{\frac{2}{n}}+\left|\frac{u_2}{\sigma_2}\right|^{\frac{2}{n}} \le \rho^{\frac{2}{n}}} \exp\left\{-k\left(\left|\frac{u_1}{\sigma_1}\right|^{\frac{2}{n}}+\left|\frac{u_2}{\sigma_2}\right|^{\frac{2}{n}}\right)\right\} du_1 du_2.$$

Similar to the previous term, first we apply the change of variables $\frac{u_1}{\sigma_1} = t_1$ and $\frac{u_2}{\sigma_2} = t_2$, and substitute the integral with 4 times the integral on the first quadrant of the coordinates. So, the integral is equal to

$$\iint\limits_{|t_1|^{\frac{2}{n}}+|t_2|^{\frac{2}{n}} \le \rho^{\frac{2}{n}}} \sigma_1\sigma_2 \exp\left\{-k\left(|t_1|^{\frac{2}{n}}+|t_2|^{\frac{2}{n}}\right)\right\} dt_1 dt_2$$
$$= 4\sigma_1\sigma_2 \iint\limits_{t_1^{\frac{2}{n}}+t_2^{\frac{2}{n}} \le \rho^{\frac{2}{n}};t_1,t_2 \ge 0} \exp\left\{-k\left(t_1^{\frac{2}{n}}+t_2^{\frac{2}{n}}\right)\right\} dt_1 dt_2.$$

Then, we apply the change of variables formula to the polar coordinate transformation $t_1 = r\cos^n\theta$ and $t_2 = r\sin^n\theta$ with $0 < r < \rho$ and $0 < \theta < 2\pi$. The Jacobean is thus

$$J = \begin{bmatrix} \dfrac{dt1}{dr} & \dfrac{dt1}{d\theta} \\ \dfrac{dt2}{dr} & \dfrac{dt2}{d\theta} \end{bmatrix}$$
$$= \begin{bmatrix} \cos^n\theta & -nr\sin\theta\cos^{n-1}\theta \\ \sin^n\theta & nr\cos\theta\sin^{n-1}\theta \end{bmatrix}$$
$$= nr\cos^{n-1}\theta\sin^{n-1}\theta,$$

Consequently,

$$4n\sigma_1\sigma_2 \int_0^{\frac{\pi}{2}}\int_0^{\rho} \exp{-kr^{\frac{2}{n}}}r\sin^{n-1}(\theta)\cos^{n-1}(\theta)drd\theta$$
$$= 4n\sigma_1\sigma_2 \int_0^{\frac{\pi}{2}} \sin^{n-1}(\theta)\cos^{n-1}(\theta)d\theta \int_0^{\rho} r\exp{-kr^{\frac{2}{n}}}dr.$$

We now substitute the first and second terms in 4.1.1 and 4.1.2 into the above relation, to obtain

$$\iint\limits_{\left|\frac{u_1}{\sigma_1}\right|^{\frac{2}{n}}+\left|\frac{u_2}{\sigma_2}\right|^{\frac{2}{n}} \le \rho^{\frac{2}{n}}} \exp\left\{-k\left(\left|\frac{u_1}{\sigma_1}\right|^{\frac{2}{n}}+\left|\frac{u_2}{\sigma_2}\right|^{\frac{2}{n}}\right)\right\} du_1 du_2.$$
$$= \frac{n^2\sigma_1\sigma_2\Gamma^2\left(\frac{n}{2}\right)}{\Gamma(n)k^n}\left[\Gamma(n) - \Gamma(n,kr^{\frac{2}{n}})\right].$$

Finally, we can obtain the close form for *K*-function as

$$K^{ESE}(\rho) = \iint\limits_{\left|\frac{u_1}{\sigma_1}\right|^{\frac{2}{n}}+\left|\frac{u_2}{\sigma_2}\right|^{\frac{2}{n}} \le \rho^{\frac{2}{n}}} g(u)du_1 du_2$$
$$= \iint\limits_{\left|\frac{u_1}{\sigma_1}\right|^{\frac{2}{n}}+\left|\frac{u_2}{\sigma_2}\right|^{\frac{2}{n}} \le \rho^{\frac{2}{n}}} \exp\left\{\sigma^2\exp\left(-\left|\frac{u_1}{\sigma_1}\right|^{\frac{2}{n}}-\left|\frac{u_2}{\sigma_2}\right|^{\frac{2}{n}}\right)\right\} du_1 du_2$$

Using Taylor expansion,

$$K^{ESE}(\rho) = \iint\limits_{\left|\frac{u_1}{\sigma_1}\right|^{\frac{2}{n}}+\left|\frac{u_2}{\sigma_2}\right|^{\frac{2}{n}}\leq\rho^{\frac{2}{n}}} \sum_{k=0}^{\infty}\frac{\sigma^{2k}}{k!}\exp\left\{-k\left(\left|\frac{u_1}{\sigma_1}\right|^{\frac{2}{n}}+\left|\frac{u_2}{\sigma_2}\right|^{\frac{2}{n}}\right)\right\}du_1 du_2$$

$$= \iint\limits_{\left|\frac{u_1}{\sigma_1}\right|^{\frac{2}{n}}+\left|\frac{u_2}{\sigma_2}\right|^{\frac{2}{n}}\leq\rho^{\frac{2}{n}}} du_1 du_2$$

$$+ \sum_{k=1}^{\infty}\frac{\sigma^{2k}}{k!}\iint\limits_{\left|\frac{u_1}{\sigma_1}\right|^{\frac{2}{n}}+\left|\frac{u_2}{\sigma_2}\right|^{\frac{2}{n}}\leq\rho^{\frac{2}{n}}}\exp\left\{-k\left(\left|\frac{u_1}{\sigma_1}\right|^{\frac{2}{n}}+\left|\frac{u_2}{\sigma_2}\right|^{\frac{2}{n}}\right)\right\}du.$$

With substitution of the three and fourth terms, 4.1.3 and 4.1.4 intop the above expression, we obtain

$$K^{ESE}(\rho) = n\sigma_1\sigma_2\rho^2\frac{\Gamma^2\left(\frac{n}{2}\right)}{\Gamma(n)} + n^2\sigma_1\sigma_2\frac{\Gamma^2\left(\frac{n}{2}\right)}{\Gamma(n)}$$
$$\sum_{k=1}^{\infty}\frac{\sigma^{2k}}{k!k^n}\left(\Gamma(n)-\Gamma(n,k\rho^2)\right).$$

Second step. Convergence of K-function.

Assume that $a_k = \frac{\sigma^{2k}}{k!k^n}\left(\Gamma(n)-\Gamma(n,k\rho^2)\right)$, and using the Ratio Test, we have

$$\lim_{k\to\infty}\left|\frac{a_{k+1}}{a_k}\right|$$

$$= \lim_{k\to\infty}\frac{\frac{\sigma^{2(k+1)}}{(k+1)!(k+1)^n}\left(\Gamma(n)-\Gamma(n,(k+1)\rho^2)\right)}{\frac{\sigma^{2k}}{k!k^n}\left(\Gamma(n)-\Gamma(n,k\rho^2)\right)}$$

$$= \lim_{k\to\infty}\frac{\sigma^2}{k+1}\times\left(\frac{k}{k+1}\right)^n\times\frac{\Gamma(n)-\Gamma(n,(k+1)\rho^2)}{\Gamma(n)-\Gamma(n,k\rho^2)}$$

$$= 0 < 1$$

Since $\lim_{k\to\infty}\frac{\sigma^2}{k+1}=0$ and $\lim_{k\to\infty}\left(\frac{k}{k+1}\right)^n=1$, we have

$$\lim_{k\to\infty}\frac{\Gamma(n)-\Gamma(n,(k+1)\rho^2)}{\Gamma(n)-\Gamma(n,k\rho^2)}$$
$$= \lim_{k\to\infty}\frac{\int_0^{\infty}t^{n-1}e^{-t}dt-\int_{(k+1)\rho^2}^{\infty}t^{n-1}e^{-t}dt}{\int_0^{\infty}t^{n-1}e^{-t}dt-\int_{kr^2}^{\infty}t^{n-1}e^{-t}dt}$$
$$= \lim_{k\to\infty}\frac{\int_0^{(k+1)r^2}t^{n-1}e^{-t}dt}{\int_0^{kr^2}t^{n-1}e^{-t}dt}$$
$$= \frac{\Gamma(n)}{\Gamma(n)} = 1.$$

Therefore, $\lim_{k\to\infty}\left|\frac{a_{k+1}}{a_k}\right| < 1$. Consequently, the series in (39) converges.

The K-function of a Poisson point process over a super-ellipse.

The pair correlation function for a Poisson point process is equal to 1. i.e, $g(u) = 1$ where u is separation vector. According to (7), the anisotropic κ-measure for Poisson point process over a bounded set A, denoted here as $\kappa_{Pois}(A)$, is given by

$$\kappa_{Pois}(A) = \int_A du.$$

Consider A as an area of a super-ellipse centred at the origin with semi-minor and semi-major axes $a = \sigma_1\rho$ and $b = \sigma_2\rho$, i.e., $A = SuE(0,a,b)$. The anisotropic K-function for a Poisson point process on A, denoted here as $K_{Pois}^{ESE}(\rho)$, is given by

$$K_{Pois}^{ESE}(\rho) = \iint\limits_{\left|\frac{u_1}{\sigma_1}\right|^{\frac{2}{n}}+\left|\frac{u_2}{\sigma_2}\right|^{\frac{2}{n}}\leq\rho^{\frac{2}{n}}} du_1 du_2.$$

Similarly to the K-function of a spatial LGCP in (39), it is easy to obtain

$$K_{Pois}^{ESE}(\rho) = n\sigma_1\sigma_2\rho^2\frac{\Gamma^2\left(\frac{n}{2}\right)}{\Gamma(n)}. \tag{40}$$

To follow the proof of (40) refer to the term 4.1.3 in the proof of (39).

References

Abrahamsen P (1997) A review of Gaussian random fields and correlation functions, Report No. 917, Sand, Norwegian computing center, Oslo, Norway

Allard D, Senoussi R, Porcu E (2016) Anisotropy models for spatial data. Math Geosci 48(3):305–328

Baddeley AJ (1999) Spatial sampling and censoring. Stoch Geom Likelihood Comput 2:37–78

Baddeley AJ, Rubak E, Turner R (2015) Spatial point patterns methodology and applications with R. CRC Press, Boca Raton

Baddeley AJ, Turner R (2005) Spatstat: an R package for analyzing spatial point patterns. J Stat Softw 12:1–42

Barndorff-Nielsen O (1977) Exponentially decreasing distributions for the logarithm of particle size. Proc R Soc Lond A Math Phys Sci 353(1674):401–419

Barndorff-Nielsen O (1978) Hyperbolic distributions and distributions on hyperbolae. Scand J Stat 5:151–157

Barndorff-Nielsen O, Halgreen C (1977) Infinite divisibility of the hyperbolic and generalized inverse Gaussian distributions. Probab Theory Relat Fields 38:309–311

Besag J (1977) Contribution to the discussion of Dr Ripley's paper. J Roy Stat Soc 39:193–195

Brix A (1999) Generalized gamma measures and shot-noise Cox processes. Adv Appl Probab 31:929–953

Christakos G (1992) Random field models in earth sciences. Academic Press, San Diego

Coles P, Jones B (1991) A lognormal model for the cosmological mass distribution. Mon Not R Astron Soc 248:1–13

Cox DR, Isham V (1980) Point Processes. CRC Press, Boca Raton

Diggle PJ (1985) A kernel method for smoothing point process data. Appl Stat 34:138–147

Diggle PJ (2013) Statistical analysis of spatial and spatio-temporal point patterns. CRC Press, Boca Raton

Diggle PJ, Moraga P, Rowlingson B, Taylor BM (2013) Spatial and spatio-temporal log-Gaussian Cox processes: extending the geostatistical paradigm. Stat Sci 28:542–563

Donoho DL (1993) Nonlinear wavelet methods for recovery of signals, densities, and spectra from indirect and noisy data, In: Proceedings of Symposia in Applied Mathematics, pp 173–205

Fuglstad GA, Lindgren F, Simpson D, Rue H (2015) Exploring a new class of non-stationary spatial Gaussian random fields with varying local anisotropy. Statistica Sinica pp 115–133

Funwi-Gabga N, Mateu J (2012) Understanding the nesting spatial behaviour of gorillas in the Kagwene Sanctuary. Cameroon Stoch Environ Res Risk Assess 26:793–811

Gao W, Li BL (1993) Wavelet analysis of coherent structures at the atmosphere-forest interface. J Appl Meteorol 32:1717–1725

Grenfell BT, Bjørnstad ON, Kappey J (2001) Travelling waves and spatial hierarchies in measles epidemics. Nature 414:716–723

Guan Y, Sherman M, Calvin JA (2004) A nonparametric test for spatial isotropy using subsampling. J Am Stat Assoc 99:810–821

Guan Y, Sherman M, Calvin JA (2006) Assessing isotropy for spatial point processes. Biometrics 62:119–125

Harper RJ, Mauger G, Robinson N, McGrath JF, Smettem KRJ, Bartle JR, George RJ (2001) Manipulating catchment water balance using plantation and farm foresty: case studies from south-western Australia, In: Nambiar EK, Brown AG (eds) Plantations, farm foresty and water, pp 44–50

Higdon D, Swall J, Kern J (1999) Non-stationary spatial modeling. In: Bernardo JM, Berger JO, Dawid AP, Smith AFM (eds) Bayesian statistics, 6. Oxford University Press, Oxford, pp 761–768

Hristopulos DT (2002) New anisotropic covariance models and estimation of anisotropic parameters based on the covariance tensor identity. Stoch Env Res Risk Assess 16(1):43–62

Hristopulos DT (2012) Statistical Models of Spatial Processes Based on Local-Interaction Energy Functionals [PowerPoint slides]. Retrieved from http://citeseerx.ist.psu.edu/viewdoc/download?doi=10.1.1.361.9705&rep=rep1&type=pdf

Illian J, Penttinen A, Stoyan H, Stoyan D (2008) Statistical analysis and modelling of spatial point patterns, vol 70. Wiley, New Jersy

Jalilian A, Guan Y, Waagepetersen R (2013) Decomposition of variance for spatial Cox processes. Scand J Stat 40:119–137

Jorgensen B (2012) Statistical properties of the generalized inverse Gaussian distribution, vol 9. Springer, Berlin

Matérn B (1960) Spatial Variation, Meddelanden fran Statens Skogsforskningsinstitut. Lecture Notes Stat 36:21

Matérn B (1986) Spatial Variation. Lecture Notes in Statistics, p 36

Mugglestone MA, Renshaw E (1998) Detection of geological lineations on aerial photographs using two- dimensional spectral analysis. Comput Geosci 24:771–784

Møller J, Rasmussen JG (2012) A sequential point process model and bayesian inference for spatial point patterns with linear structures. Scand J Stat 39:618–634

Møller J, Syversveen AR, Waagepetersen R (1998) Log Gaussian Cox processes. Scand J Stat 25:451–482

Møller J, Toftaker H (2014) Geometric anisotropic spatial point pattern analysis and Cox processes. Scand J Stat 41:414–435

Møller J, Waagepetersen R (2003) Statistical inference and simulation for spatial point processes. CRC Press, Boca Raton

Neyman J, Scott EL (1958) Statistical approach to problems of cosmology. J R Stat Soc B 20:1–29

Ohser J (1983) On estimators for the reduced second moment measure of point processes. Math Operationsforschung Stat Ser Stat 14:63–71

Ohser J, Stoyan D (1981) On the second-order and orientation analysis of planar stationary point processes. Biom J 23:523–533

Perry EC, Velazquez-Oliman G, Marin L (2002) The hydrogeochemistry of the karst aquifer system of the northern Yucatan Peninsula. M Int Geol Rev 44:191–221

Redenbach C, Sarkka A, Freitag J, Schladitz K (2009) Anisotropy analysis of pressed point processes. Adv Stat Anal 93:237–261

Ripley BD (1976) The second-order analysis of stationary point processes. J Appl Probab 13:255–266

Rosenberg MS (2004) Wavelet analysis for detecting anisotropy in point patterns. J Veg Sci 15:277–284

Schlather M, Malinowski A, Menck PJ, Oesting M, Strokorb K (2015) Analysis, simulation and prediction of multivariate random fields with package RandomFields. J Stat Softw 63:1–25

Schlather M (1999) Introduction to positive definite functions and to unconditional simulation of random fields, Tech. Rep. ST-99-10, Departament of Mathematics and Statistics, Faculty of Applied Sciences, Lancaster University, UK

Serra L, Saez M, Juan P, Varga D, Mateu J (2014) A spatio-temporal Poisson Hurdle point process to model wildfires. Stoch Env Res Risk Assess 28:1671–1684

Thomas M (1949) A generalization of Poisson's binomial limit for use in ecology. Biometrika 36:18–25

Uria J, Ibanez R, Mateu J (2013) Importance of habitat heterogeneity and biotic processes in the spatial distribution of a riparian herb (Carex remota L.): a point process approach. Stoch Environ Res Risk Assess 27:59–76

Wallace A (1968) Differential topology. Benjamin/Cummings, Reading, MA, USA

Wolpert RL, Ickstadt K (1998) Poisson/gamma random field models for spatial statistics. Biometrika 85:251–267